Astron. Astrophys. 261, 18–24 (1992)

ASTRONOMY AND ASTROPHYSICS

The radio structure of extended quasars

I. A VLBI survey of the nuclear emission

J.R.A. Hooimeyer[1], P.D. Barthel[2], R.T. Schilizzi[1,3], and G.K. Miley[1]

[1] Leiden Observatory, P.O. Box 9513, NL-2300 RA Leiden, The Netherlands
[2] Kapteyn Astronomical Institute, University of Groningen, P.O. Box 800, NL-9700 AV Groningen, The Netherlands
[3] Netherlands Foundation for Research in Astronomy, P.O. Box 2, NL-7990 AA Dwingeloo, The Netherlands

Received September 19, 1991; accepted January 27, 1992

Abstract. Snapshot VLBI observations at 5 GHz have been obtained for a subset of a sample of 30 quasars with extended radio structure. For all but one of the 12 sources involved, the objects were detected at one or more baselines. In 9 quasars, the visibility data revealed the presence of resolved core structure. Model-fitting indicated the nuclear emission of these sources to be quasi-linear and, in most cases, of core–jet type. Spearman rank correlations show that, for the total sample of 30 extended quasars, the projected radio size, the degree of jet curvature and the lobe arm length asymmetry are strongly correlated with the radio core luminosity, in the sense predicted by relativistic beaming models; they are *un*correlated with the relative core strength R, however. Follow-up observations of both pc-scale and overall radio morphologies of those quasars having resolved milliarcsec-scale structure are described in a companion paper.

Key words: interferometry – quasars – radio sources: general

1. Introduction

In the past decade, considerable effort and observing time has been spent in the mapping and monitoring of the nuclei of large double-lobed radio sources, mostly quasars, with very long baseline interferometry (VLBI) techniques. The most powerful incentive for this intense study of lobe-dominated quasars was provided by the belief that VLBI monitoring of these sources would offer a crucial test for the relativistic beaming hypothesis. In beaming models (Rees 1966; Blandford & Königl 1979; Orr & Browne 1982; Pearson & Zensus 1987), large lobe-dominated radio sources are presumed to be the unbeamed counterparts of compact superluminal sources such as 3C 273, seen at large inclination angles to the line of sight. If this hypothesis were correct, then large lobe-dominated sources would be expected to display superluminal motion very rarely or never, and to have more symmetrical, less distorted radio structure than compact radio sources, on both milli-arcsec (mas) and larger scales. Detection of superluminally expanding core components in a large fraction of quasars with extended radio structure would effectively rule out simple versions of the relativistic beaming model.

Several samples of lobe-dominated quasars are now being studied with VLBI by various groups (e.g. Barthel et al. 1984; Zensus & Porcas 1986; Hough & Readhead 1989). Since 1980 our collaboration has been investigating the mas-structure of a sample of quasars selected from the Hewitt and Burbidge optical QSO catalogue (Burbidge et al. 1977; Hewitt & Burbidge 1980, 1987) by the strength and extent of their radio emission. The applied selection criteria were: 1) known extended radio structure, with a largest angular size exceeding 10 arcsec, 2) known redshift, 3) $\delta_{1950.0} > 0°$, 4) a core flux density at 5 GHz exceeding 100 mJy. The latter two criteria were included to ensure reasonable UV-coverage and sufficient sensitivity using the available VLBI networks. The sample thus selected on the basis of radio extent and core flux density, consists of 30 extended (but not exclusively lobe-dominated) quasars.

The core flux density limit adopted here has been introduced mainly to improve our chances of actually finding observable nuclear radio emission. The lower limit imposed on the quasar core fluxes may create a bias towards the inclusion of sources aligned along small inclinations θ with the line of sight: the extended sources under consideration here have relative core intensities R which on average are roughly a factor of 5 higher than is the case for extended quasars in general. However, we believe any orientation bias that may have been introduced by this core flux density criterion to be compensated by the demand that the selected sources should be of large angular (and linear) extent. To illustrate this, we compare the linear size distribution of our sample with that of the 3CR sample. The low-frequency selected 3CR sample (Spinrad et al. 1985; Djorgovski et al. 1987) contains mostly steep-spectrum, double-lobed radio sources with weak radio cores (low R) which are believed to be largely free of orientation bias selection effects (Hough & Readhead 1987, 1989). Figure 1 shows the linear projected size distribution of our sample and that of the 3CR quasars within the same redshift range (0.2–1.7). The 3CR quasars are systematically smaller than our objects; the two distributions differ at a significance level of 97% in a one-tailed Kolmogorov–Smirnov test. In the context of the Orr & Browne (1982) model, the observed size distributions imply that the survey quasars generally have radio structures closer to the plane of the sky than the 3CR quasars. Thus, if the claim that

Send offprint requests to: G.K. Miley

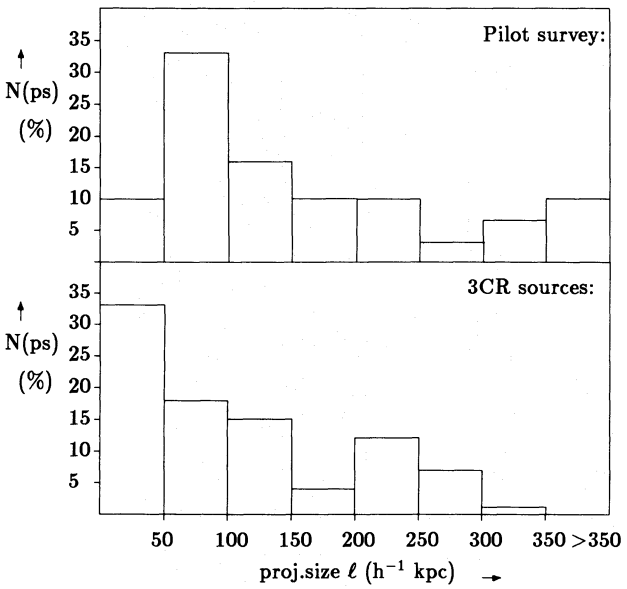

Fig. 1. The distribution of linear projected size l for the 30 sources in our survey, and for the 3CR sources within the same redshift range (0.2–1.7)

the 3CR sample is randomly oriented in space (e.g. Hough & Readhead 1987) is correct, the survey quasars are likely to be inclined farther away from the line of sight than quasars on average are. Many of the survey objects are among the largest quasars known. It is unlikely that these huge sources will be inclined preferentially close to the line of sight. On these grounds, we consider the objects in our sample to be oriented close to the plane of the sky, despite the adopted core flux density limit.

Our original sample, compiled in 1980 from the Burbidge et al. (1977) catalogue, consisted of 18 triple quasars, satisfying the flux and size criteria defined above. A pilot survey of these sources was carried out in a global VLBI experiment at 5 GHz, the observations and results of which are described in detail in Barthel et al. (1984). At a later stage, twelve other quasars were selected from the more recent Hewitt & Burbridge (1980) catalogue, using the same criteria, and added to the sample. A second pilot survey of these twelve objects was carried out in October 1984, the results of which will be described below.

In Sect. 2 the observations and data reduction are described. Section 3 reviews the results for each individual source. In Sect. 4 the general characteristics of the mas-scale structures for the entire sample are presented. Section 5 contains some concluding remarks. In 13 of the 30 quasars in the sample as a whole, evidence was found for the presence of resolved nuclear structure on pc-scales. Follow-up observations of the central and overall radio morphologies of these objects have been obtained with VLBI networks and the Very Large Array (VLA). These experiments are described in a companion paper (Hooimeyer et al. 1991; henceforth HSMB).

2. Observations and data reduction

The observations of the second survey were carried out during 12–14 October 1984 in a trans-Atlantic VLBI experiment at 5 GHz. The six telescopes involved were those at Effelsberg, Medicina, Onsala, Haystack, Green Bank and Owens Valley.

Table 1. The elements in the interferometer system

Telescope	Diameter (m)	T_{sys} (K)	sensitivity (K Jy^{-1})
Effelsberg	100	60	1.45
Medicina	32	55	0.18
Onsala	26	35	0.06
Haystack	36	70	0.16
Green Bank	43	45	0.27
Owens Valley	40	55	0.27

Parameters of the interferometer system are given in Table 1. The most relevant properties of the twelve sources observed are summarized in Table 2, including references to maps of their large scale radio structure in the literature. In the conversion from angular to linear sizes, cosmological parameters $H_o = 100h$ km s^{-1} Mpc^{-1} and $q_o = 0.05$ have been assumed (values used throughout this paper). The conditions under which the observations took place were not ideal. During part of the observing run the Effelsberg and Haystack telescopes suffered from receiver problems, while strong winds made observing at Onsala difficult.

For each source three or four short scans of about 15 min duration each were made at different hour angles. The coherent integration time usually was 2 min, but for some weak sources had to be increased up to 6 min. Left-circular polarization was used. The data were recorded using the standard Mk II recording system with 2 MHz bandwidth. Cross-correlation of the data was carried out at the California Institute of Technology (Caltech) in Pasadena. The correlated flux scale was calibrated according to Cohen et al. (1975), assuming the calibrators 0235+164, 2134+004 and OJ287 to be unresolved at the shorest spacings.

The source structures have been analyzed by model-fitting the correlated visibility amplitudes and phases. Models containing one, two or three Gaussian components were fitted to the data in an iterative χ^2 procedure. Iteration was stopped when no further improvement in the agreement of the model with the fringe visibilities could be achieved by varying one or more of the model parameters. Greatest weight was given to the data on the longest baselines. In some cases this resulted in models fitting the long baselines well, but with some flux density missing on the shortest spacings. For a few sources enough data points were available to attempt making a crude hybrid map in addition to, and as an independent check on, the model-fits. For this purpose the Cornwell & Wilkinson (1981) mapping algorithm and the Caltech VLBI software package have been used.

Parameters of the model-fits are given in Table 3. Due to the sparseness of visibility data, for most sources the uncertainties in the model parameters are large. The error values quoted for the parameters in Table 3 have been derived both by estimates "by eye", and from χ^2-fits to the visibility data. The error ranges listed in the table represent the mean values of these two methods.

The detected mas-scale structures of the twelve quasars have been classified into three categories: core–jet structure (i.e. containing one flux-dominant component, with secondary components of much lower intensity to one side of it); resolved symmetric structure (the fringe amplitudes of one or more baselines definitely vary in the course of time, while the visibility phases and

Table 2. The sample of the second pilot survey

IAU name	Other	z	S_{tot}^{5000} (mJy)[a]	S_{core}^{5000} (mJy)[a]	R[b]	LAS (″)	l (h^{-1} kpc)	Ref.
0850+581	4C 58.17	1.322	1400	910	1.03	15	90	1,2
1011+232	4C 23.24	0.565	830	750	6.85	16	53	2,3
1022+194	4C 19.34	0.828	760	580	2.11	48	130	2
1055+201[c]	4C 20.24	1.110	1110	870	2.15	62	330	5
1111+408	3C 254.0	0.734	790	110	0.11	13	65	2,4
1150+497	4C 49.22	0.334	1120	320	0.33	21	33	3,4
1218+339	3C 270.1	1.519	1000	220	0.15	10	62	3
1229−021	4C-02.55	1.038	1020	380	0.36	18	100	2
1317+520	4C52.27	1.060	720	270	0.36	29	165	2,4,5
1602−001	PKS	1.625	450	200	0.41	20	125	3,6
1830+285	4C 28.45	0.594	1070	370	0.38	28	125	2,5
2209+080	4C 08.64	0.484	1090	300	0.29	16	65	2,5
2251+134	4C 13.85	0.677	790	560	1.70	13	50	2,5

[a] The errors in the quoted flux density values are typically 10–20 mJy.
[b] R has been defined as S_{core}/S_{ext}, divided by $(1+z)^{\alpha}$, where a value of 0.7 has been assumed for α.
[c] Source was included in the first survey (Barthel et al. 1984), but has been re-observed after sudden core brightening.
References to large-scale structure: 1. Browne (1987), 2. Hintzen et al. (1983), 3. Shone (1985), 4. Owen & Puschell (1984), 5. Hooimeyer et al. (1991) (HSMB), 6. Barthel et al. (1988).

Table 3. Parameters of model fits/hybrid maps

Source	VLA core flux[b] (mJy)	VLBI flux total[a, b]	(mJy) core[b]	Structure	Size/separation[c] (mas)	Pos. angle (°)
0850+581	885	880	640	core–jet	4.5±0.5	168±2
1011+232	720	720	410	core–jet	4.5±0.5	−165±5
1022+194	690	580	490	core–jet	3.5±0.5	38±4
1055+201	870	710	500	resolved	3±1	0±5
1111+408	110	<40	<40	undetected	—	—
1150+497	390	380	180	core–jet	6±1	135±3
1218+339	220	160	?	?	—	—
1229−021	400	180	?	?	—	—
1317+520	350	350	120	core–jet	6±1	125±4
1602−001	200	180	?	?	—	—
1830+285	370	360	300	core–jet	2.5±0.5	−28±2
2209+080	300	300	290	resolved	3±1	0±6
2251+134	570	520	390	resolved	3±1	57±5

[a] Correlated fringe amplitude on shortest available baseline.
[b] Typical error values are 20–50 mJy for the VLBI flux densities and 10–20 mJy for the VLA core flux densities.
[c] For core–jet sources: separation between primary and secondary component. For resolved sources without clear multiple component structure: FWHM of the Gaussian that gives the best fit to the visibilities.

model-fits do not indicate the presence of asymmetric structure); and structure unknown (i.e. available data too scarce to allow the determination of a self-consistent model). No unresolved mas-scale structures were detected in this second pilot survey.

3. Results for individual sources

0850+581: High signal-to-noise maps of the large-scale structure of this bright, slightly distorted triple quasar can be found in Hintzen et al. (1983), Shone (1985) and Barthel et al. (1986). In the 1984 VLBI observations the strong nuclear emission of 0850+581 was easily detected on all baselines. Model-fits of the correlated amplitudes and phases, and the subsequent hybrid mapping, indicated the source to be resolved. The nuclear emission shows the core–jet morphology typical of powerful quasars. A secondary component is present at a distance of 4.5 ±1.0 mass from the 700 mJy core, at a position angle of roughly 170°. The VLBI structure appears to join smoothly with the

curved inner part of the distorted kpc-scale radio jet. Observations carried out at later epochs (1985, 1986) in the context of the strong source survey by Pearson & Readhead (1988) have shown superluminal expansion to occur in the secondary component of 0850+581, at a velocity of $\sim 2.5\,h^{-1}\,c$ (Barthel et al. 1986). These higher signal-to-noise observations confirm the basic nuclear morphology present in these survey data.

1011+232: A 1.4 GHz VLA map of the large-scale radio emission of this small, somewhat distorted and moderately variable quasar can be found in Hintzen et al. (1983). In the present VLBI observations, the source was detected on all three available baselines: Medicina-Green Bank, Medicina–Owens Valley and Green Bank–Owens Valley. The closure phases are clearly offset from zero, indicating the presence of asymmetric structure on mas-scales. Model-fitting yields a core–jet structure, with a 230 mJy secondary component at ~4.3 mas from the 550 mJy core, along a position angle of approximately −165°. The pc-scale emission is on the same side as, and closely aligned to, the inner part of the kpc-scale radio jet.

1022+194: This S-shaped, edge-darkened quasar is dominated by its nuclear radio emission (Hintzen et al. 1983). The quasar has been selected in our sample on the grounds of its large angular extent (48 arcsec, corresponding to a linear projected size of $130\,h^{-1}$ kpc). The VLBI snapshot observations resulted in strong detections on all available baselines. As in 1011+232, the closure phases are systematically offset from zero. The mas-scale radio structure is slightly resolved; modelfits and hybrid mapping indicated the presence of a 420 mJy core and a 40 mJy secondary at ~3.5 mas and position angle ~40°. Again, the VLBI structure is in the direction of, and nearly collinear with, the large scale radio jet.

1055+201: This large triple quasar, which has been mapped by Hintzen et al. (1983) and HSMB, is a variable radio source, showing occasional outbursts. Shortly before the VLBI observations of October 1984, the source underwent a small flare, in which the core brightened by ~50%. In earlier VLBI observations (Barthel et al. 1984), the source was unresolved at 5 GHz, implying the angular size of the core to be less than 1 mas. In our present observations, however, the VLBI core is definitely resolved and ≈4 mas in size. Apparently, mas-structure has developed in the time interval between the two observations. Strong detections were found on all baselines. The modelfits and hybrid map indicate a resolved linear structure, nearly 4 mas in angular extent. The resolved festure is directed north–south, and as such is closely aligned with the outer lobe structure.

1111+408: Maps of the large-scale structure of this source have been published by Hintzen et al. (1983) and Owen & Puschell (1984). The quasar has a strongly asymmetric double radio structure, with a largest angular size of ~15″ and a straight, steep radio spectrum ($\alpha_{178}^{5000} \approx -0.95$; Véron-Cetty & Véron 1989). The source was not detected in the present VLBI observations. This puts an upper limit of 30–40 mJy on the correlated flux density of the mas-scale radio emission.

1150+497: This powerful quasar is included in the S5 1 Jy catalogue of Kühr et al. (1981). Arcsec-resolution maps of 1150+497 have been published by Shone (1985) and Owen & Puschell (1984). Mas-scale core emission was detected on all available baselines in the present observations, and was found to be clearly resolved. Amplitudes and phases could be fitted with a core–jet model: a 130 mJy secondary component is present at a distance of 6 mas along a position angle of roughly 135° of the 250 mJy core. Thus, the VLBI structure is aligned to within a few degrees with the inner part of the prominent, curved 50 kpc radio jet.

1218+339: With its angular size of 10 arcsec, this is the smallest quasar in our sample. It has a triple radio structure, aligned nearly north–south (Shone 1985; Stocke et al. 1985). In the present survey, the quasar was detected only on the two shortest and most sensitive baselines: Effelsberg–Medicina and Green Bank–Owens Valley, with correlated flux densities of 160 and 140 mJy, respectively. Too few data were available to get an indication of the mas-scale structure.

1229−021: The radio morphology of this quasar is straight and triple (Hintzen et al. 1983), and asymmetric in the sense that the lobe on the jet side is much closer to the core than the other lobe. The emission of the mas-core at 5 GHz is weak: there was a detection on only one baseline, Green Bank–Owens Valley (flux density 180 mJy). The nuclear radio emission therefore probably is rather diffuse.

1317+520: The large-scale radio structure of this curved triple quasar, which is approximately 30 arcsec in extent, has been described by Hintzen et al. (1983), Owen & Puschell (1984) and HSMB. On VLBI scales, the radio structure is clearly resolved. Model-fitting and hybrid mapping yield a linear, apparently symmetric three-component structure along a position angle of ~125°. This is roughly in the direction of the southern radio jet (position angle 134°). The strongest of the three components is the central one, the other two features being of roughly equal flux density. The closure phases do not appear to be systematically offset from zero, which is another indication that the observed structure is indeed symmetric. If so, the nucleus of 1317+520 would be an exception among powerful quasar cores. High signal-to-noise multi-frequency VLBI observations maps will be required to determine the exact position of the (flat-spectrum) VLBI core component.

1602−001: This relatively weak quasar has the highest redshift in our sample: $z = 1.625$. It has a classical triple structure 20 arcsec in angular size, aligned nearly east–west. A very faint jet travels outwards to the western lobe (Shone 1985; Barthel et al. 1988). The nucleus is one of the weakest in our sample, with a VLA 5 GHz core flux density of ~210 mJy. In the survey, 1602−001 was detected only on the three shortest and most sensitive baselines, with correlated fluxes ranging from 110 to 180 mJy. The available data were too scarce and noisy to allow us to determine whether the core emission was resolved or not.

1830+285: This powerful source has a triple radio structure, with a prominent, clumpy jet extending to the northwestern lobe. VLA maps of 1830+285 have been obtained by Hintzen et al. (1983) and HSMB. In the VLBI survey, the source was detected on all baselines. The nuclear emission of 1830+285 shows the familiar core–jet structure, with a secondary component located at ~2.5 mas from the core, along a position angle of ~−30°. Some weak, diffuse emission may be present at larger distances from the nucleus. Common to what is usually observed in lobe-dominated objects of similar morphology, the misalignment between pc- and kpc-scale radio emission is small (~5°).

2209+080: This bright, low-declination quasar, which is included in the S5 catalogue of Kühr et al. (1981), has a triple radio structure, aligned nearly north–south (Hintzen et al. 1983, HSMB). The nuclear emission of 2209+080 is rather variable in strength: the VLA core flux density at 5 GHz has ranged from 100 to 350 mJy in the period 1983–1988 (HSMB). In the October 1984 observations the core was detected clearly on all baselines, with flux densities ranging from 70 to 300 mJy. The nuclear structure appears to be resolved in the north–south direction, and well aligned with the large-scale jet emission. Due to the relatively low declination of 2209+080 and the partial filling of the *uv*-plane, the convolving beam is rather elongated ($\sim 10 \times 1$ mas) in this direction, smearing the north–south structure. Thus, although the visibilities indicate the source to have resolved mas-scale structure, we cannot distinguish individual features in the map. A single elliptical Gaussian of 3×1 mas provides an adequate fit to the limited data.

2251+134: Maps of the large-scale radio structure of this optically faint quasar can be found in Hintzen et al. (1983) and HSMB. Its curved, S-shaped morphology is reminiscent of models of precession of the source axis. In the survey, fringes were easily detected on all baselines. The source is resolved at mas-scales. The correlated closure phases are not systematically offset from zero, signalling that strongly asymmetric core–jet structure cannot be present. Model-fitting and hybrid mapping both indicate the presence of symmetrical structure of a few mas in size, elongated in the direction of the inner part of the kpc-scale jet. This orientation of the mas-scale structure is consistent with an interpretation of the source morphology in terms of precession of the radio axis.

4. Properties of the sample as a whole

Together, the two pilot surveys contain 30 extended quasars, listed in Table 4. Columns 1 and 2 contain the source names and the redshift z. Column 3 contains the total luminosity $L_{\rm tot}^{5000}$ at 5 GHz. Column 4 gives the relative core strength R, which has

Table 4. Radio properties of the sample quasars

Source	z	log ($L_{\rm tot}^{5000}$) (W Hz)	log R	l (h^{-1} kpc)	A	Ref.	mas-scale structure	ΔPA (°)	C (°h kpc^{-1})
0003+158	0.450	26.54	−0.18	112	0.1	1	R	3	0.059
0214+108	0.408	26.52	−0.27	399	0.1	1	R	—	0.017
0610+260	0.580	27.50	−0.48	232	0.1	2, 12	R	1	0.038
0742+318	0.462	26.96	0.86	532	0.1	4, 5	CJ	3	0.013
0836+195	1.692	27.60	−0.15	61	0.9	6, 15	U	—	—
0838+133	0.684	27.52	−0.20	262	0.1	7	U	—	—
0850+581	1.322	28.25	0.27	89	0.2	8	CJ	7	1.933
0855+143	1.048	27.78	−0.58	53	0.0	6	U	—	0.151
0932+022	0.659	26.85	−0.36	162	0.7	1, 10	CJ	4	0.453
1011+232	0.565	27.23	1.02	53	0.2	9, 10	CJ	3	0.940
1022+194	0.828	27.49	0.52	130	0.0	10	CJ	17	0.675
1040+123	1.029	28.02	−0.46	43	0.1	8, 10, 16	CJ	13	0.315
1047+096	0.786	27.11	0.77	315	0.9	1, 10	—	—	0.573
1055+201	1.110	27.96	0.57	330	0.2	9, 12	CJ	11	0.164
1058+110	0.420	26.29	−0.53	105	0.0	1	—	—	0.
1111+408	0.734	27.39	−1.17	64	0.1	3, 10	—	6	0.246
1137+660	0.652	27.41	−0.68	204	0.3	8	CJ	3	0.062
1150+497	0.334	26.78	−0.41	33	0.1	3, 9	CJ	5	1.252
1203+109	1.088	27.43	0.43	34	0.2	1, 10	—	—	1.453
1218+339	1.519	28.25	−0.55	62	0.9	9, 10, 17	D	—	0.931
1222+216	0.435	27.05	−0.01	68	0.1	4, 10	CJ	23	5.601
1229−021	1.038	27.85	−0.23	99	0.7	10	D	—	0.588
1317+520	1.060	27.72	−0.21	165	0.3	3, 10, 12	CJ	9	0.535
1548+114	0.436	26.69	0.30	190	0.1	10, 12	CJ	3	0.070
1602−001	1.625	27.98	−0.10	123	0.1	9, 15	D	—	0.178
1618+177	0.555	27.04	−0.71	210	0.2	1, 6, 10	U	—	0.174
1721+343	0.206	26.18	−0.05	667	0.1	13, 14	CJ	4	0.010
1830+285	0.594	27.31	−0.28	125	0.0	10, 12	CJ	5	0.219
2209+080	0.484	27.12	−0.80	65	0.3	10, 12	R	9	0.368
2251+134	0.677	27.30	−0.80	50	0.3	10, 12	R	25	0.280

References to large-scale structure: 1. Miley & Hartsuyker (1978), 2. Riley & Pooley (1975), 3. Owen & Puschell (1984), 4. Neff (1982), 5. Fanti et al. (1977), 6. Jenkins et al. (1977), 7. Pooley & Henbest (1974), 8. Browne (1987), 9. Shone (1985), 10. Hintzen et al. (1983), 11. Laing (1981), 12. Hooimeyer et al. (1991) (HSMB), 13. Barthel (1987), 14. Jägers et al. (1982), 15. Barthel et al. (1988), 16. Foley & Barthel (1990), 17. Stocke et al. (1985).

been defined as the ratio $L_{\rm core}^{5000}/(L_{\rm tot}^{5000}-L_{\rm core}^{5000})$, divided by a K-correction factor $(1+z)^{\alpha}$, where a value of 0.7 has been adopted for α ($S_\nu \sim \nu^{-\alpha}$). Column 5 contains the linear projected radio size l. Column 6 lists the lobe asymmetry A, which has been defined as the ratio $(E1-E2)/(E1+E2)$, where $E1$ and $E2$ are the distances respectively from the farthest and nearest lobes to the core. Column 7 contains references to the large-scale radio structure of the source. Column 8 gives a reference to the structure of the mas-core: "U" indicates an unresolved core, "CJ" a core–jet morphology, "R" a resolved, apparently symmetric structure, "–"a non-detection. "D" indicates that the source has been detected but that insufficient data were available to deduce the source structure. Column 9 lists the misalignment angle ΔPA between the pc-scale VLBI structure and the *inner* part of the kpc-scale radio jet. Finally, column 10 gives the curvature C; this parameter has been defined as the total angle through which the quasar jet apparently bends from core to outer lobe, divided by the length of the jet (in h^{-1} kpc).

One of the most notable results of the two surveys is the high detection rate of mas-scale emission: 27 out of 30 quasars have been detected on at least one baseline. Most of the core flux observed in arcsec-scale maps is seen on the (shortest) VLBI baselines, i.e. it is contained within a region of several tens of mas. The pc-scale cores of these triple quasars therefore are quite compact.

For the sources for which enough data were available to yield a fairly reliable impression of the mas-scale structure present, no evidence was found for complex radio structures; at the limited dynamic range available, the derived structures are either unresolved or linear. In some cases the emission appears to be symmetric, in the sense that features are detected on both sides of the brightest component. However, only by multi-frequency observations can it be determined whether the mas-scale structure in these objects is truly asymmetric or of core–jet type. In all cases where asymmetric structure appears to be present, the secondary VLBI component and the kpc-scale jet are on the same side of the dominant core component. In general, the mas-scale structure joins smoothly with the arcsec-scale jet; the median value of ΔPA is only $5\pm3°$. Spearman rank correlations have been carried out between the various luminosity and morphology parameters. An overview of the most relevant results is given in Table 5. For each set of parameters are tabulated the Spearman rank correlation coefficients, the number of observations and the probability p that the observed correlation could have arisen by chance. A correlation is considered to be significant when $p<10\%$.

Inspection of Table 4 shows that the misalignments between the small- and large-scale jets tends to be highest for the smallest and/or most distorted quasars in the sample. The objects with the most strongly curved jets are systematically smaller and have brighter cores than less distorted quasars. This is in qualitative agreement with what is expected in the context of the relativistic beaming model (Orr & Browne 1982). The jet curvature C, however, is not significantly correlated with the relative core strength R. This is not likely to be an artifact caused by a limited range in R or C, since both R and C span over two orders of magnitude.

R is not related significantly to projected radio size l, either. This may imply that linear radio size and jet curvature are not determined solely, or to a decisive degree, by orientation effects. The lobe asymmetry A is correlated significantly with redshift z, in the sense that high-redshift quasars have larger values of A. A similar result was found by Barthel & Miley (1988) for a much larger sample of steep-spectrum quasars with a greater range in redshift ($z<3$), but there the dependence of A upon z only became significant at redshift values higher than contained in our sample ($z>1.5$–2). This effect may, as Barthel & Miley argue, be caused by cosmological evolution of the density of the interstellar medium in quasars: at earlier epochs the interstellar matter is postulated by them to be more dense, and hence better able to distort or stop the radio jet. A clumpy, uneven gas distribution could then result in strongly curved and asymmetric jet emission. However, the apparent correlation between A and z may also be due to a mutual dependence on a third parameter: both lobe length asymmetry and redshift are correlated significantly with the radio luminosities $L_{\rm tot}$ and $L_{\rm core}$. In a flux-limited sample such as the one considered here, redshift and luminosity effects are hard to separate, and it is not possible to distinguish which of the two is primarily responsible for the behaviour of lobe asymmetry.

Table 5. Spearman rank correlations

Correlation	Corr. coeff.	p	Number of objects
l–z	−0.28	0.13	30
l–$L_{\rm tot}$	−0.33	0.07	30
l–$L_{\rm core}$	−0.27	0.14	30
l–$L_{\rm ext}$	−0.35	0.06	30
l–R	0.17	0.36	30
A–z	0.40	0.04	30
A–$L_{\rm core}$	0.33	0.07	30
A–$L_{\rm ext}$	0.22	0.25	30
A–R	0.07	0.70	30
ΔPA–z	0.22	0.11	25
ΔPA–$L_{\rm core}$	0.46	0.04	25
ΔPA–$L_{\rm ext}$	0.31	0.17	25
ΔPA–R	0.15	0.52	25
C–z	0.26	0.12	25
C–$L_{\rm tot}$	0.28	0.13	25
C–$L_{\rm core}$	0.40	0.03	25
C–$L_{\rm ext}$	0.18	0.32	25
C–R	0.17	0.36	25
C–α_{1400}^{5000}	−0.47	0.009	25
l–ΔPA	−0.47	0.03	25
l–curv.	−0.58	0.001	25
ΔPA–curv.	0.57	0.007	25
A–curv.	0.37	0.07	25

5. Conclusions

We have described the results of preliminary observations of the pc-scale radio emission in the nuclei of large double-lobed quasars. At the limited dynamic range of the pilot survey observations, the nuclear radio structure of these powerful objects is generally found to be linear and directed towards the large-scale radio jet, with which it joins smoothly. No complicated nuclear morphologies were detected, nor was there any evidence for gross

misalignments between pc- and kpc-scale emission. In these two respects, the mas-scale structure of extended quasars differs markedly from that observed in many steep-spectrum compact sources, such as 3C 147, 3C 216 and 0153+744 (Pearson et al. 1987; Browne 1987).

Statistically, morphological parameters such as core-dominance R, projected linear size l and misalignment ΔPA, on the whole exhibit trends which are consistent with the predictions of beaming models. Not too much importance should be attached to this, in view of the incompleteness of the sample under study. The main result of importance regarding the beaming hypothesis is the fact that the apparent side-to-side flux density asymmetry which is ubiquitously observed in the nuclei of compact flat-spectrum sources, appears to be generally present in the nuclei of these large triple quasars as well; but strictly speaking, multi-frequency VLBI observations are required to establish this apparent one-sidedness of the mas-scale radio emission definitely.

Acknowledgements. We thank the staff at the telescopes involved in this experiment for their assistance with the observations. We are grateful to the correlator staff at the California Institute of Technology for their help with the data processing. The Netherlands Foundation for Research in Astronomy is supported by the Netherlands Organization for Scientific Research (NWO).

References

Barthel P.D., Miley G.K., Schilizzi R.T., Preuss E., 1984, A&A 140, 399
Barthel P.D., Pearson T.J., Readhead A.C.S., Canzian B.J., 1986, ApJ 310, L7
Barthel P.D., 1987, in: Pearson T.J., Zensus J.A. (eds.) Superluminal Radio Sources. p. 148
Barthel P.D., Miley G.K., 1988, Nat. 333, 319
Barthel P.D., Miley G.K., Schilizzi R.T., Lonsdale C.J., 1988, A&Supp. 73, 515
Barthel P.D., 1989, ApJ 336, 601
Blandford R.D., Königl A., 1979, ApJ 232, 34
Blumenthal G.R., Keel W., Miller J.S., 1982, ApJ 257, 499
Browne I.W.A., 1987, in: Zensus J.A., Pearson T.J. (eds.) Superluminal Radio Sources. p. 129
Burbidge G., Crowne A., Smith H.E., 1977, ApJS 33, 113
Cohen M.H., Moffet A.H., Romney J.D., Schilizzi R.T., Shaffer D.B., Kellermann K.I., Purcell G.H., Grove G., Swenson G.W., Yen J.L., Pauliny-Toth I.I.K., Preuss E., Witzel A., Graham D., 1975, ApJ 210, 249
Cornwell T.J., Wilkinson P.N., 1981, MNRAS 196, 1067
Djorgovsky S., Spinrad H., Pedelty J., Rudnick L., Stockton A., 1987, AJ 93, 1307
Fanti C., Fanti R., Formiggini L., Lari C., Padrielli L., 1977, A&Supp. 28, 351
Foley A.R., Barthel P.D., 1990, A&A 228, 17
Hewitt A., Burbidge G., 1980, ApJS 43, 57
Hewitt A., Burbidge G., 1987, ApJS 63, 1
Hintzen P., Ulvestad J., Owen F.N., 1983, AJ 88, 709
Hooimeyer J.R.A., Schilizzi R.T., Miley G.K., Barthel P.D., 1991, A&A (submitted) (HSMB)
Hough D.H., Readhead A.C.S., 1987, ApJ 321, L11
Hough D.H., Readhead A.C.S., 1989, AJ 98, 1208
Jägers W.J., Van Breugel W.J.M., Miley G.K., Schilizzi R.T., Conway R.T., 1982, A&A 105, 278
Jenkins C.J., Pooley G.G., Riley J.M., 1977, Mem. Roy. Astron. Soc. 84, 61
Kühr H., Witzel A., Pauliny-Toth I.I.K., Nauber U., 1981, A&AS 45, 36
Laing R.A., 1981, MNRAS 195, 261
Miley G.K., Hartsuyker A., 1978, A&AS 34, 129
Neff S.G., 1982, Ph.D. Thesis, Univ. of Virginia
Orr M.J.L., Browne I.W.A., 1982, MNRAS 200, 1067
Owen F.N., Puschell J.J., 1984, AJ 89, 932
Pearson T.J., Readhead A.C.S., Barthel P.D., 1987, in: Zensus J.A., Pearson T.J. (eds.) Superluminal Radio Sources. p. 94
Pearson T.J., Readhead A.C.S., 1988, ApJ 328, 114
Pearson T.J., Zensus J.A., 1987, in: Zensus J.A., Pearson T.J. (eds.) Superluminal Radio Sources. p. 1
Pooley G.G., Henbest S.N., 1974, MNRAS 169, 477
Rees M.J., 1966, Nat. 211, 468
Riley J.M., Pooley G.G., 1975, Mem. Roy. Astron. Soc. 80, 105
Scheuer P.A.G., 1987, in: Zensus J.A., Pearson T.J. (eds.) Superluminal Radio Sources. p. 104
Shone D., 1985, Ph.D. Thesis, Univ. of Manchester
Spinrad H., Djorgovsky S., Marr J., Aguilar L., 1985, PASP 97, 932
Stocke J.T., Burns J., Christiansen W., 1985, ApJ 299, 799
Véron-Cetty M.P., Véron P., 1989, ESO Scient. Report no. 7
Wills B.J., Browne I.W.A., 1986, ApJ 302, 56
Zensus J.A., Porcas R.W., 1986, in: Swarup G., Kapahi V.K. (eds.) Proc. IAU Symp. 119, Quasars

Astron. Astrophys. 261, 25–40 (1992)

ASTRONOMY AND ASTROPHYSICS

The radio structure of extended quasars

II. The radio emission on pc- and kpc-scales

J.R.A. Hooimeyer[1], R.T. Schilizzi[1,2], G.K. Miley[1], and P.D. Barthel[3]

[1] Leiden Observatory, P.O. Box 9513, NL-2300 RA Leiden, The Netherlands
[2] Netherlands Foundation for Research in Astronomy, P.O. Box 2, NL-7990 RA Dwingeloo, The Netherlands
[3] Kapteyn Astronomical Institute, University of Groningen, P.O. Box 800, NL-9700 AV Groningen, The Netherlands

Received September 19, 1991; accepted January 27, 1992

Abstract. VLBI and VLA observations of the nuclear and overall radio structures are presented for eight quasars possessing large double-lobed radio emission. On milli-arcsec scales, the nuclei of five sources show an asymmetric (core–jet) morphology, one has a symmetric appearance, one is unresolved and one is too weak to allow a reliable determination of its structure. Total intensity, polarization and spectral index maps of the associated kpc-scale emission were obtained for six of the eight quasars. The inner and outer radio jet emission generally are well aligned and pointing in the same direction; in one source, the pc- and kpc-scale jet are oppositely directed. Jet velocities close to the hot spots were estimated for several quasars from the intensity of their hot spot emission. The velocity estimates were relativistic in all cases (ranging from 0.5 to 0.9 c).

Key words: interferometry – quasars: general – radio sources: general

1. Introduction

Powerful radio sources show a great diversity in radio morphology and spectral behaviour. The well-known relativistic beaming model (Blandford & Königl 1979; Scheuer & Readhead 1979; Orr & Browne 1982) has proven remarkably successful in explaining this variety of observational characteristics in terms of the orientation of relativistically expanding jet material. The mapping and monitoring of the milliarcsec (mas) scale emission in the nuclei of large lobe-dominated sources has long been considered to provide a vital observational test to the beaming hypothesis (e.g. Scheuer 1984). Since, within the context of the beaming model, these objects are hypothesized to lie in or close to the plane of the sky, their core emission should exhibit symmetrical (not one-sided) structure, and subluminal, or at best mildly superluminal, expansion. Detection of significant superluminal motion or systematically asymmetric nuclear radio structure in a large fraction of lobe-dominated sources should present strong evidence against the simple Orr and Browne model. This idea triggered the setup of several very long baseline interferometry (VLBI) monitoring projects of large samples of lobe-dominated sources.

Since the early eighties, our group has been involved in studying the radio characteristics of a sample of 30 quasars with large double-lobed structure. These sources were selected from the optical QSO catalogue of Hewitt & Burbidge (1980) on the basis of their angular radio extent and their nuclear radio luminosity. We chose to concentrate on extended quasars with bright radio cores, rather than on a randomly oriented sample of objects including many weak nuclei; this allowed us to obtain mas-scale structural information for a complete sample of double-lobed quasars within a limited amount of observing time. The large physical sizes of the selected sources should help ensure that they are oriented at large angles to the line of sight (see discussion in Hooimeyer et al. 1991; henceforth HBSM).

A preliminary VLBI survey, the results of which have been described in Barthel et al. (1984) and HBSM, yielded evidence for the presence of resolved structure on mas scales in 13 of the 30 sources. Two of these, the quasars 1137+660 (3C 263) and 1150+497 (4C 49.22) have been studied by other investigators (Zensus & Porcas 1986; Linfield, unpublished). The remaining 11 sources have been observed by us with global VLBI networks at 5 GHz. For three of the 11 quasars, the sources 0610+260, 0742+318 and 1721+343, observations have already been published elsewhere (Barthel et al. 1985, 1989). First-epoch VLBI maps of the remaining eight sources will be presented and discussed in this article. For six of these sources, additional observations of the associated large scale radio structure have been obtained at 5 and 15 GHz with the very large array (VLA; Thompson et al. 1980). Section 2 describes the observations and the data reduction. In Sect. 3, the VLBI and VLA data are presented and discussed for each quasar individually. Subsequently, a comparison is made between the morphologies of the pc-scale nuclear structure (presumed to be due to recent activity) and the overall morphology of the extended quasars (produced by integrated activity over 10^7 yr). This should give us a better insight in the evolution of the radio jets in these large objects. An estimate of jet velocities in extended quasars close to the radio lobes can be obtained from the luminosity and energy density of the hot spot emission. In Sect. 5, jet velocities in the vicinity of the lobes are estimated for several extended quasars. Finally, in Sect. 6 the most relevant results are summarized, and their implications discussed briefly.

Send offprint requests to: G.K. Miley

2. Observations and data reduction

2.1. VLBI observations

At 5 GHz, the nuclei of all eight extended quasars could be mapped using the Mk II recording system. Observations of the eight quasars have been made with global VLBI networks at 5 GHz during the period 1985–1988. A journal of the observations is shown in Table 1. The quantity and quality of the data varied considerably. For five quasars (0850+581, 1317+520, 1548+114, 1830+285, 2251+134) a full 12 h coverage could be obtained; for the sources 1055+201, 1222+216 and 2209+080 the observing runs were of shorter duration. Source switching was applied between 1055+201 and 1222+216.

All experiments were carried out using standard Mk II recording equipment at 2 MHz bandwidth. Left circular polarization was recorded. The data were correlated using the 5- and 10-stations Mk II correlators at the California Institute of Technology (Caltech) in Pasadena, and then coherently averaged over 2–4 min. For the weakest objects, 2209+080, 1548+114 and 1830+285, global fringe fitting was applied (Schwab & Cotton 1983). The correlated data were reduced using the Caltech VLBI and AIPS software packages. Flux calibration was performed following Cohen et al. (1975), assuming the primary calibrators to be unresolved on all baselines. The usual self-calibration and hybrid mapping procedures were applied (e.g. Pearson & Readhead 1984). An overview of the derived model parameters is presented in Table 2. The values quoted for component flux, separation and position angle represent a weighted mean of the values determined by the model fitting and hybrid mapping procedures. Errors in these numbers have been estimated by visual inspection and reduced χ^2 values for the agreement between model and observed visibilities.

2.2. VLA observations

Low-frequency radio maps of arcsec resolution (at 1400 and 408 MHz) of the eight quasars which we have studied with VLBI, have been published by Hintzen et al. (1983), Owen & Puschell (1984), and Shone (1985). Our objective was to obtain supplementary high signal-to-noise maps of these sources at higher frequency and resolution. For two of the eight quasars, detailed VLA and MERLIN maps of high quality have been made by other observers: 0850+581 (Shone 1985) and 1222+216 (Neff, private communications). The remaining six objects have been mapped by ourselves with the VLA in its B-configuration at 5 and 15 GHz, and a bandwidth of 50 MHz. The resolution achieved at these frequencies is $\sim$1 and 0.3″, respectively. Total intensity (I) and linear polarization (P) maps were derived for all sources at both frequencies.

The observations were carried out in August 1986 in snapshot mode; two or three scans of $\sim$15 min duration each were taken of each object at various hour angles. Every source scan was preceded and succeeded by a short ($\sim$1–2 min) observation of a nearby secondary calibrator source. An absolute flux density level was established using several short observations of the primary VLA flux calibrator 3C 48. Calibration of the instrumental polarization was achieved by repeated observation of 3C 286 at various parallactic angles. Atmospheric disturbances due to a local thunderstorm affected some of the 15 GHz scans. A sufficient amount of data was left to derive high signal-to-noise intensity maps for all six objects, but the noise in the 15 GHz polarization maps is relatively high.

The data were reduced using the standard AIPS reduction software. For each source, maps of the four Stokes parameters I, Q, U and V were obtained at 5 and 15 GHz. From these, maps of the spectral index α_5^{15}, the linear polarized intensity P, and the distribution of the electric vector ϕ were derived. The integrated flux densities, linear polarizations and polarization position angles are given for all quasars in Table 3. Table 3 further contains several morphological parameters of the large-scale radio emission, such as the angular extent, the jet–counterjet flux density ratio f and the jet–counterjet length asymmetry A. (A has been defined as $(E_1-E_2)/(E_1+E_2)$, where E_1 and E_2 are the distances from the quasar core to the farthest and nearest hot spot or lobe centroid, respectively.)

Flux densities, linear polarization levels and spectral index values were also determined for the main substructures in each source: core, jet, lobe and hot spots. These values are listed in

Table 1. Observing log

Source	Other name	VLA		VLBI		
		Observed date	Frequency (GHz)	Observed date	Duration (h)	Telescope name
0850+580	4C 58.17	—	—	01/06/86	12	SBWL-KG
1055+201	4C 20.24	14/7/86	5.15	01/06/86	6	SBWL-KG
1222+216	4C 21.35	—	—	01/06/86	6	SBWL-KG
1317+520	4C 52.27	14/7/86	5.15	01/10/87	12	SBWLJ-G
1548+114	4C 11.50	14/7/86	5.15	25/09/87	12	SBWLJ-G
1830+285	4C 28.45	14/7/86	5.15	02/06/86	12	SBWL-KG
2209+080	4C 08.64	15/7/86	5.15	02/06/86	6	SBWL-KG
2251+134	4C 13.85	15/7/86	5.15	27/09/85	12	SBWLJ-K
				02/06/86[b]	6	SBWL-KG

[a] Abbreviations of station names: S = Onsala (26 m), B = Effelsberg (100 m), W = WSRT (14 × 25 m), L = Medicina (32 m), J = Jodrell Bank (76 m), K = Haystack (36 m), G = Green Bank (43 m), Y = VLA (27 × 25 m), O = Owens Valley (40 m).
[b] 2251+134 re-observed.

Table 2. Parameters of VLBI CLEAN model components

Source	Component	Flux (mJy)	Distance (mas)	Position angle (°)	Size (mas)
0850+581	A	638±2	0.0	0	0.4±0.1
	B	99±2	1.1±0.1	161±1	0.4±0.1
	C	7±1	4.1±0.1	140±1	1.1±0.1
	D	6±1	6.1±0.1	155±1	0.7±0.1
	E	5±1	12.2±0.1	146±3	2.3±0.1
1055±201	A	516±2	0.0	0	0.2±0.1
	B	75±4	2.2±0.1	−6±1	0.4±0.1
	C	85±4	2.1±0.1	174±1	0.7±0.1
1222±216	A	360±1	0.0	0	0.8±0.1
	B	18±1	3.3±0.1	−15±1	0.5±0.1
	C	7±1	7.2±0.1	−12±1	0.8±0.1
1317+520	A	108±2	0.0	0	0.8±0.1
	B	21±1	4.7±0.1	125±1	0.8±0.1
	C	8±1	6.1±0.1	126±1	0.8±0.1
	D	5±1	8.3±0.1	135±2	0.8±0.1
1548+114	A	310±1	0.0	0	0.3±0.1
	B	12±1	1.4±0.1	69±4	0.6±0.1
1830+285	A	312±1	0.0	0	0.6±0.1
	B	25±2	2.1±0.1	−37±1	0.5±0.1
	C	21±2	3.9±0.1	−33±1	0.5±0.1
2209+080	A	148±4	0.00	0	3×1
2251+134	A	370±2	0.0	0	0.5±0.1
	B	62±2	1.8±0.1	39±2	0.8±0.1
	C	54±1	2.5±0.1	−138±2	1.0±0.1

Table 3. Integrated radio parameters

Source	15 GHz		5 GHz				
	Flux (mJy)	% pol.	Flux (mJy)	% pol.	LAS[a] (″)	A[a]	f[b]
1055+201	862	0.7	1370	2.5	62	0.2	—/—
1317+520	245	1.3	491	11.2	29	0.3	4.6/24
1548+114	231	0.0	402	0.2	46	0.1	6.0/45
1830+285	482	1.8	780	4.1	28	0.0	6.0/35
2209+080	305	4.2	628	6.7	16	0.3	4.0/90
2251+134	792	0.0	948	2.9	13	0.3	1.5/—

[a] Measured from lowest frequency map.
[b] Quoted values of jet–counterjet flux density ratios for 5 and 15 GHz, respectively.

Table 4. Minimum energy densities u_{min} and equipartition magnetic field values B_{eq} were determined under the usual assumptions of cylindrical symmetry, energy equipartition between relativistic particles and the magnetic field, and a filling factor of unity (Miley 1980). The luminosity of the individual components has been calculated using $H_0 = 100h$ km s^{-1} Mpc^{-1} and $q_0 = 0.05$.

3. Notes on individual sources

3.1. 0850+581

This distorted triple radio source contains one of the brightest radio cores in our sample; strictly speaking, it is not a lobe-dominated object. Because of its high radio luminosity, 0850 +581 has been included in the bright source survey of Pearson &

Table 4. Derived parameters for source components

Component	S_5 (mJy)	% pol. P_5	S_{15} (mJy)	% pol. P_{15}	α_5^{15}	u_{min} (erg cm^{-3})	B_{eq} (G)
1055+201							
Core	1067	2.4	685	0.7	0.4	$6.7\,10^{-8}$	$8.3\,10^{-4}$
Jet	38	—	—	—	—	—	—
N lobe[a]	232	0.5	96	0.5	0.7	$1.7\,10^{-10}$	$0.4\,10^{-4}$
Hot spot	132	0.5	65	0.5	0.65	$9.9\,10^{-9}$	$4.4\,10^{-4}$
S lobe	35	—	—	—	—	$1.4\,10^{-10}$	$0.4\,10^{-4}$
1317+520							
Core	316	10.7	190	1.2	0.45	$3.2\,10^{-8}$	$5.7\,10^{-4}$
Jet	26	3.4	7	—	1.15	$1.6\,10^{-10}$	$0.4\,10^{-4}$
NW lobe	21	2.4	—	—	>2.0	$1.5\,10^{-11}$	$1.2\,10^{-5}$
SE lobe[a]	128	5.8	46	0.9	0.90	$1.2\,10^{-10}$	$3.5\,10^{-5}$
Hot spot	89	4.9	41	0.9	0.80	$0.9\,10^{-10}$	$3.2\,10^{-5}$
1548+114							
Core	339	<0.5	231	—	0.35	$1.5\,10^{-8}$	$3.9\,10^{-4}$
Jet	12	<0.5	—	—	—	$0.4\,10^{-10}$	$0.2\,10^{-4}$
SE lobe	5	<0.2	—	—	—	$1.7\,10^{-12}$	$4.2\,10^{-6}$
NW lobe[a]	48	<0.5	—	—	—	$5.1\,10^{-12}$	$7.2\,10^{-6}$
Hot spot	42	1.0	—	—	—	$4.0\,10^{-9}$	$2.0\,10^{-4}$
1830+285							
Core	592	—	423	—	0.30	$2.7\,10^{-8}$	$5.2\,10^{-4}$
Jet	31	—	12	—	0.85	$7.7\,10^{-11}$	$2.8\,10^{-5}$
SE lobe	35	—	10	—	1.15	$1.1\,10^{-10}$	$1.1\,10^{-5}$
NW lobe[a]	115	4.0	37	1.7	1.0	$3.0\,10^{-11}$	$1.8\,10^{-5}$
Hot spot	60	4.0	32	1.7	0.50	$2.4\,10^{-9}$	$2.6\,10^{-4}$
2209+080							
Core	235	5.8	190	1.2	0.20	$1.4\,10^{-8}$	$3.8\,10^{-4}$
N lobe	99	1.5	25	—	1.25	$1.3\,10^{-10}$	$3.5\,10^{-5}$
S jet	110	2.4	57	—	0.60	$0.3\,10^{-9}$	$5.5\,10^{-5}$
S lobe[a]	69	1.8	18	—	1.20	$1.8\,10^{-10}$	$4.3\,10^{-5}$
Hot spot	25	1.7	9	—	0.90	$0.9\,10^{-9}$	$1.8\,10^{-4}$
2251+134							
Core	648	4.7	730	—	−0.1	$3.6\,10^{-8}$	$6.0\,10^{-4}$
NE lobe+jet	137	—	25	0.8	1.5	$0.9\,10^{-10}$	$3.2\,10^{-5}$
SW jet	52	2.9	16	—	1.05	$7.3\,10^{-10}$	$8.7\,10^{-5}$
SW lobe	111	2.1	19	—	1.60	$3.4\,10^{-10}$	$5.8\,10^{-5}$

[a] Total lobe emission, including hot spot regions.

Readhead (1984), and as such it already had been observed with VLBI at several epochs, for a few hours at a time, prior to the present observations. It has since then been discovered to be a superluminal source (Barthel et al. 1986).

We have not obtained arcsec-resolution observations of this source. A high signal-to-noise MERLIN map of the large-scale radio structure of 0850+581 is shown in Shone (1985) and Browne (1987). Here we present VLBI observations of the nuclear emission of 0850+581.

At epoch 1986.42, 0850+581 was tracked by an 8-station network for a full 12 h. The resulting map is shown in Fig. 1a. The mas-scale radio structure is dominated by a bright northern component, containing approximately 85% of the total flux in the map. On the grounds of its relative brightness and its flux variability, we assume this component (designated A in Fig. 1) to be the quasar core. Secondary resolved components, B and C, are located at 4.4 and 6.3 mas to the southeast of A, and a weak resolved feature D is present at roughly 11 mas distance. The visibilities on the shortest baselines further indicate the presence of ~10 mJy of diffuse emission at distances of 20–30 mas from the core, beyond the boundaries of the man displayed in Fig. 1, and aligned along a position angle 178±4°. The three features B, C, and D were detected in the earlier maps of Barthel et al. (1986). In addition, a new component A′, close to the core, has become apparent, which was not present in previous maps; meanwhile, the central component A itself has decreased in flux density by ~15% compared to the value quoted by Barthel et al. for their last epoch 1985.77. The mas-scale structure is not perfectly collinear, and appears to "wiggle" on the scale of a few mas. The newly discovered component A′ is elongated along a position

angle of $174 \pm 4°$ with respect to the core A, whereas the more distant components B, C and D are resolved along position angles of 164 ± 2, 162 ± 2 and $168 \pm 3°$, respectively. On kpc scales the radio jet of 0850+581 displays a similar "cork–screw" behaviour (Barthel et al. 1986). The wiggle of the jet on mas and arcsec scales is consistent with an interpretation in terms of precession of the radio axis.

When compared with the data of Barthel et al., the 1986.42 map of 0850+581 confirms the presence of superluminal motion in this quasar. In Fig. 1b the distance of components B and C with respect to the core A is plotted versus time. A weighted least-squares fit through the data of the three epochs of Barthel et al. (1986) and the 1986.42 data yield a proper motion $\mu_{B,C} = 0.11 \pm 0.02$ mas yr^{-1}. At a redshift $z = 1.322$ and using $H_0 = 100h$, $q_0 = 0.05$, this value corresponds to an apparent expansion velocity $\beta_{app} = (4.8 \pm 0.7)h^{-1}c$, which is equal to within the errors to the value of $(5.3 \pm 0.8)h^{-1}c$ given by Barthel et al.

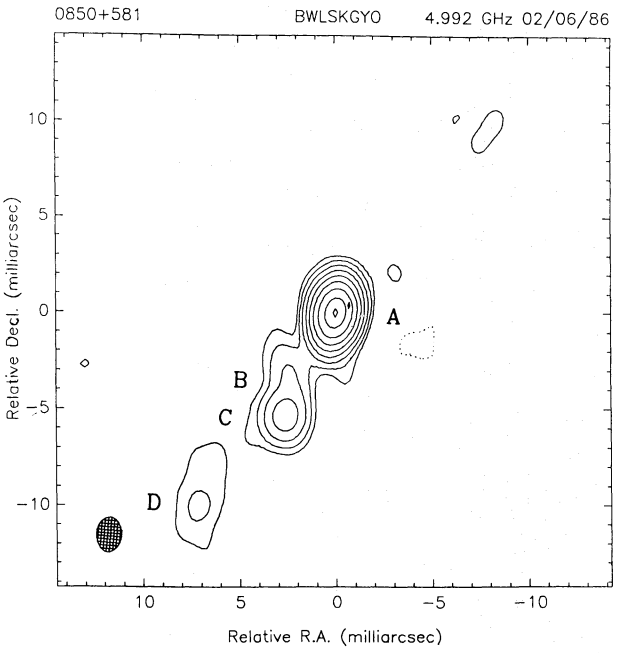

Fig. 1a. 5 GHz VLBI map of the total intensity I of 0850+581, observed at epoch 1986.42. The contour levels in the map are 0.2, 0.5, 1, 2, 4, 8, 16, 32, 64 and 96% of the peak flux value of 649 mJy per beam. The restoring beam is an ellipse of 1.8×1.2 mas, at a position angle of $-5°$

3.2. *1055+201*

(*a*) *Mas-scale radio structure*: In the earliest VLBI observations of this large double-lobed radio source (Barthel et al. 1984), the mas-scale nuclear emission was unresolved at 5 GHz, implying an angular core size smaller than 1 mas. In the middle of 1984, however, 1055+201 underwent a radio flare, in which the core brightened by approximately 50%. Subsequent VLBI snapshot observations indicated the nuclear radio emission to be resolved at 5 GHz, and roughly 4 mas in size (HBSM).

Figure 2a shows the map of the radio core of 1055+201 obtained in June 1986. The quality of these data was low. The experiment suffered from station failures and very poor tape playback performance. Also, source switching between 1055+201 and another source resulted in large gaps in the *uv*-coverage. The best fit to the visibilities was obtained by a triple structure 4×0.7 mas in size, oriented along a position angle of $-6°$ (i.e. in the direction of the northern radio lobe). The two outer features are both considerably weaker than the central component, and of roughly equal flux density.

Attempts during the mapping procedure to force the clean-component model towards an asymmetric mas-scale structure, resulted in appreciably worse fits of the model to the visibility amplitudes and phases. Also, the closure phases do not show any systematic offset from zero within the errors, which is further evidence that the symmetry in the map is real. However, the noise in the phase data is large on the weaker baselines, so that the possibility that the observed symmetry is an artifact caused by phase errors cannot be excluded.

(*b*) *Large-scale radio structure*: The large, double-lobed radio source associated to 1055+201 is dominated by a bright, flat

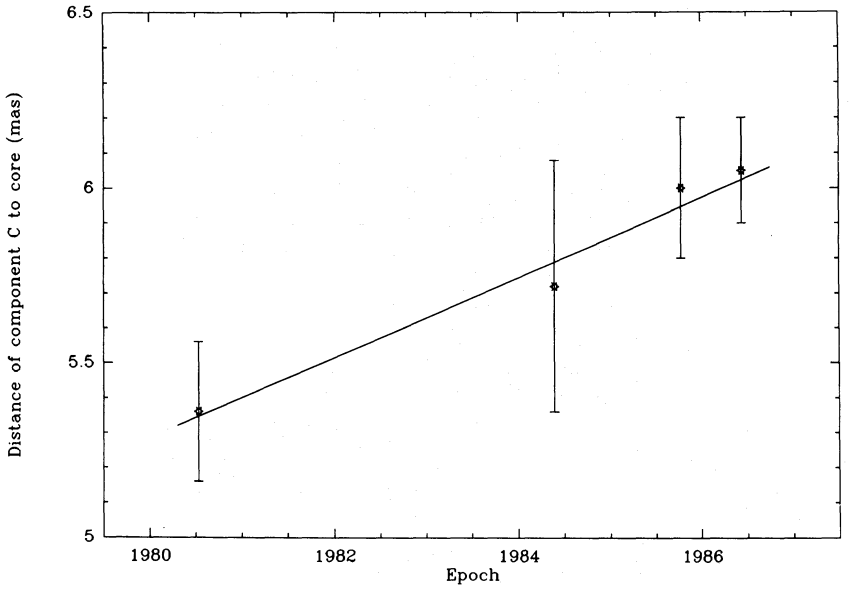

Fig. 1b. The distance of components B and C with respect to the presumed core A as function of time. Data points and error bars of the epochs preceding 1986.42 have been taken from Barthel et al. (1986); the data from epoch 1986.42 have been taken from the present map. The solid line represents a weighted least-squares fit through the data of component B, the dashed line the same for component C. The proper motions implied by the two fits are $\mu_B = 0.11 \pm 0.02$ and $\mu_C = 0.12 \pm 0.02$ mas yr^{-1}, respectively

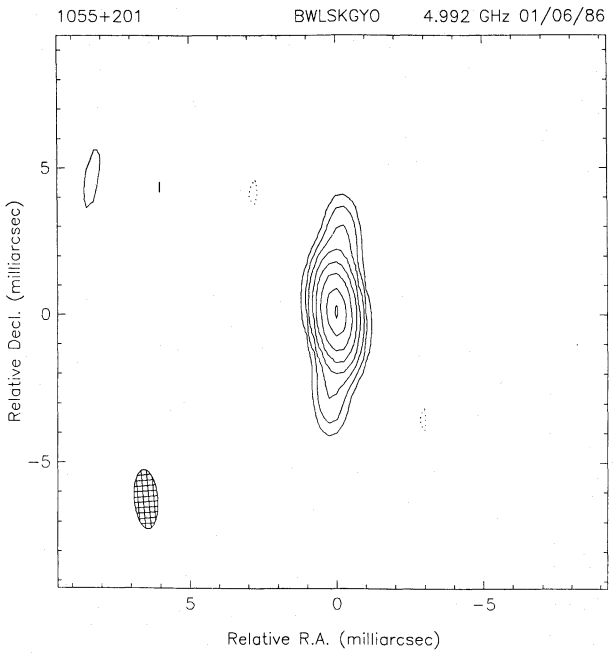

Fig. 2a. 5 GHz VLBI map of the total intensity I of 1055+201, observed at epoch 1986.42 in source switching mode with 1222+216. The contour levels in the map are 0.5, 1, 2, 4, 8, 16, 32, 64 and 96% of the peak flux value of 591 mJy per beam. The restoring beam is an ellipse of 2.0 by 1.0 mas, at a position angle of 8°

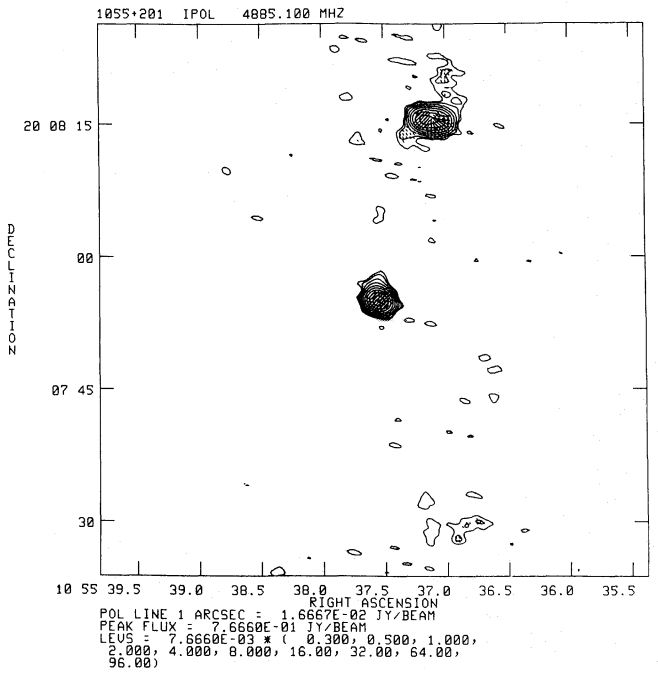

Fig. 2b. VLA map of the total intensity distribution I of 1055+201 at 5 GHz. The contour values in the map are 0.35, 0.5, 1, 2, 4, 8, 16, 32, 64 and 96% of the peak flux value of 766.6 mJy per beam. Superimposed on the contour plot are the electric vectors of the linearly polarized emission P, scaled in length to the intensity of P. An electric vector 1″ in size corresponds to a polarized flux density of 10 mJy per beam

spectrum core ($\alpha_5^{15} \sim -0.4$, using the convention $S_\nu \propto \nu^{-\alpha}$). At 15 GHz, almost all of the flux in the map originates from the core. The emission from the northern lobe is faint; the southern lobe is undetectable. The 15 GHz map is therefore not shown here. At 5 GHz (Fig. 2b), the nucleus of 1055+201 contains ~80% of the total flux density of the source. In the 5 GHz map, slight extensions can be seen to the north of the core and to the south of the northern lobe, but otherwise there is no trace of a large scale radio jet in the 5 and 15 GHz maps.

The bright northern lobe has a complex morphology. In the 5 GHz map of Fig. 2b the lobe emission is clearly resolved in the east-west direction. In our 15 GHz data and in a higher dynamic range 15 GHz map by Owen (private communication), the northern lobe contains a double hot spot structure, the two peaks being linked by a ridge of emission. The surrounding diffuse lobe emission is extended mainly to the north of the two hot spots, away from the core. The hot spot structure and the connecting bridge are oriented nearly perpendicular to the radio source axis. The weak extension to the southeast of the lobe visible in the 5 GHz map suggests that the kpc-scale jet terminates close to the brightest, eastern hot spot. The part of the jet visible in the map in the vicinity of the primary hot spot is linearly polarized at a level of 1%, with the electric vector field running parallel to the jet direction. In the hot spot region the magnetic field becomes circumferential. The primary hot spot has a somewhat higher degree of polarization and flatter spectrum than the secondary, western one. The lobe emission south of the nucleus is diffuse and of low surface brightness. In the low signal-to-noise 1.4 GHz VLA map of 1055+201 published by Hintzen et al. (1983), the southern lobe was not visible, but in deeper 1.4 GHz maps the weak southern emission has been detected clearly (Ulvestad, private communication). In the present 5 GHz map the intensity of the southern lobe emission is barely above the noise level. The linear polarization and the spectral index behaviour of this feature could not be determined with reliability.

3.3. 1222+216

On arcsec scales, this relatively small quasar (with a linear projected radio size of $45h^{-1}$ kpc) possesses a highly distorted triple radio structure (Hintzen et al. 1983; Neff, private communication), with a jet curved over more than 130°. The VLBI map derived from the June 1986 experiment, is shown in Fig. 3. The *uv*-coverage obtained in this observation, was severely limited due to source switching with another source, and to loss of data because of poor tape playback quality. The mas-scale nuclear radio emission consists of a "core–jet"-type structure, oriented nearly north-south, in the direction of the large scale jet. The dominant (~360 mJy) component, A, is assumed to be the radio core; model fitting indicates a secondary component B to be positioned at ~3.3 mas distance, along position angle = −15°, closely aligned with the MERLIN jet (Neff, private communication). A weaker, resolved feature C is present at ~7 mas to the northeast of A. "Missing" flux density on the shortest baselines, unaccounted for by the model, further indicates the presence of some diffuse, extended emission on scales of 20–30 mas, in the region to the northwest of the core.

3.4. 1317+520

(*a*) *Mas-scale radio structure*: On mas scales, the nucleus of this triple quasar displays a curved multi-component radio structure

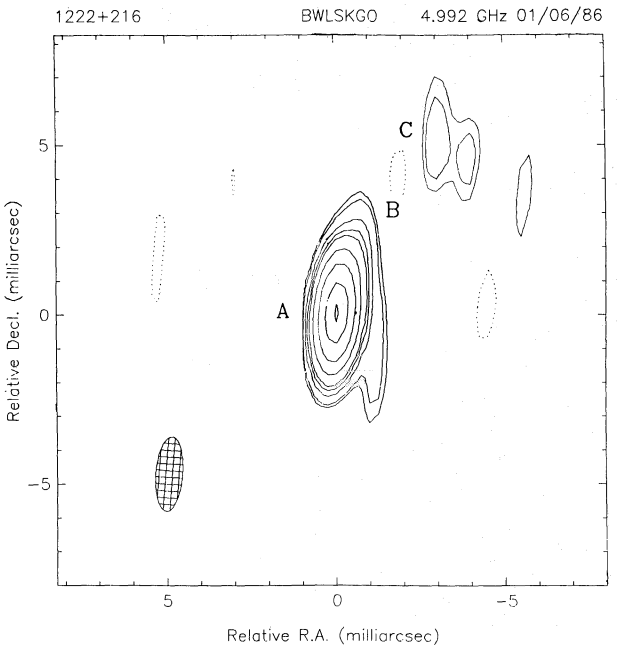

Fig. 3. 5 GHz VLBI map of the total intensity I of 1222+216, observed at epoch 1986.42 in source switching mode with 1055+201. The contour levels in the map are 0.75, 1, 2, 4, 8, 16, 32, 64 and 96% of the peak flux value of 352 mJy per beam. The restoring beam is an ellipse of 3.0 by 0.8 mas, at a position angle of −8°

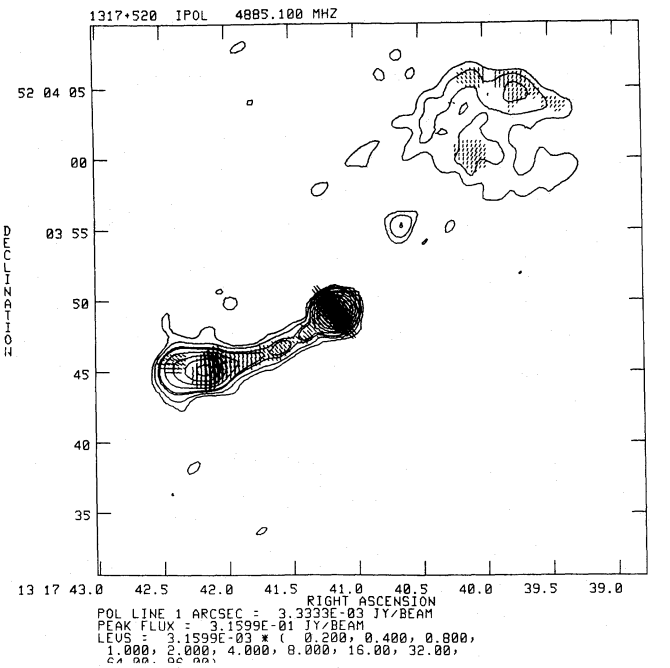

Fig. 4b. VLA map of the total intensity distribution I of 1317+520 at 5 GHz. The contour values in the map are 0.2, 0.4, 0.8, 1, 2, 4, 8, 16, 32, 64 and 96% of the peak flux value of 316.0 mJy per beam. Superimposed on the contour plot are the electric vectors of the linearly polarized emission P, scaled in length to the intensity of P. An electric vector 1″ in size corresponds to a polarized flux density of 3.3 mJy per beam

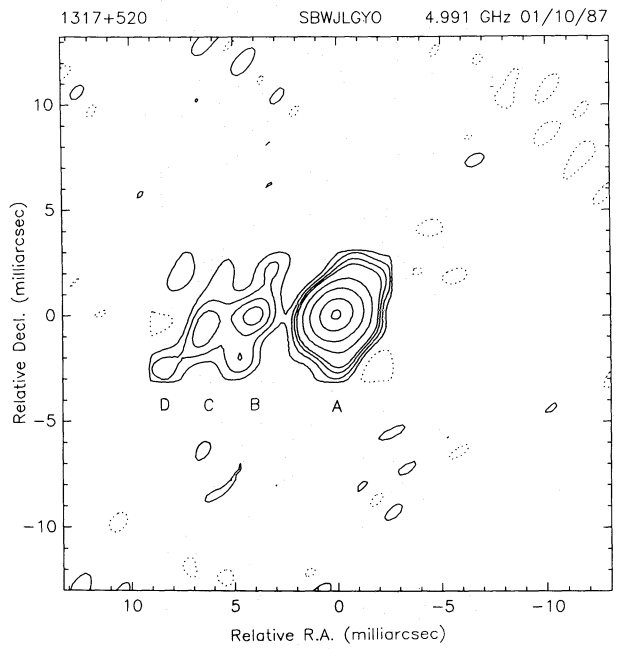

Fig. 4a. 5 GHz VLBI map of the total intensity I of 1317+520, observed at epoch 1987.76. The map has been rotated clockwise over an angle of 35°. The contour levels in the map are 1, 2, 4, 8, 16, 32, 64 and 96% of the peak flux value of 115 mJy per beam. The restoring beam is an ellipse of 1.5 × 0.6 mas, at a position angle of 9°

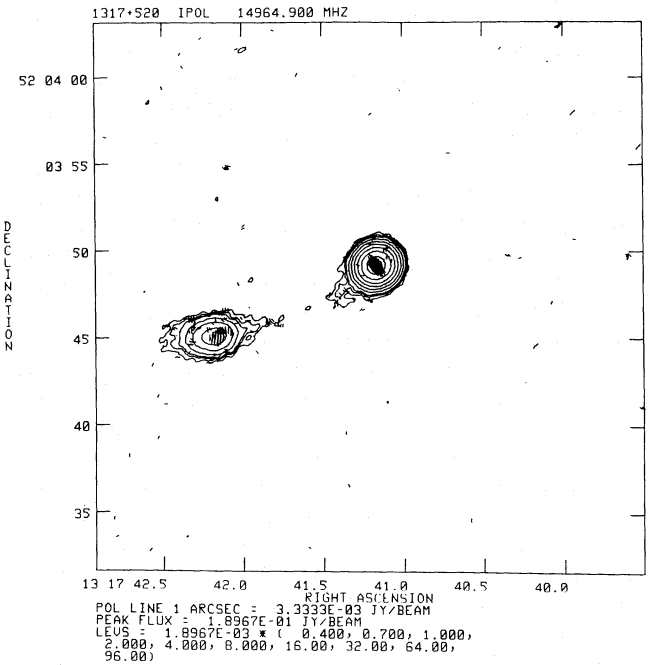

Fig. 4c. VLA map of the total intensity distribution I of 1317+520 at 15 GHz. The contour values in the map are 0.4, 0.7, 1, 2, 4, 8, 16, 32, 64 and 96% of the peak flux density of 190.0 mJy per beam. Superimposed on the contour plot are the electric vectors of the linearly polarized emission P, scaled in length to the intensity of P. An electric vector 1″ in size corresponds to a polarized flux density of 3.3 mJy per beam

(Fig. 4a). At least four separate components, designated A, B, C and D from west to east, can be discerned. Additionally, a small amount of diffuse emission (~ 5 mJy) is present at larger distances (~ 30 mas) from the nucleus.

The brightest, somewhat resolved, component in the hybrid map, A, is assumed to be the core. The mas-scale core–jet structure then is asymmetric in the same sense as the large scale VLA jet (Fig. 4b, c). In view of the possible presence of counterjet emission on kpc scales (see below), an unambiguous spectral identification of the core position by means of VLBI observations at other frequencies is desirable.

The nuclear "jet" curves from east to south; the outer radio jet is seen to curve back again to the east. This morphology is consistent with models involving jet precession.

(*b*) *Large-scale radio structure*: The arcsecond-scale radio structure of 1317+520 is shown in Fig. 4b, c. In the 5 GHz map (Fig. 4b) a bright, continuous jet is seen to extend from the core to the southwest. At $\sim 8''$ from the nucleus, the jet spreads out into a fairly narrow lobe structure, containing a single, intense flux density peak. Both the lobe and the hot spot are elongated in the direction of the slightly curved jet. The hot spot is located at the end of the lobe closest to the radio core. In the 15 GHz map the southern jet emission is very weak, implying a steep radio spectrum for this component: $\alpha_5^{15} \geq 1.5$. At the central knot in the jet $\sim 4''$ from the core the spectrum is slightly flatter ($\alpha = 1.1$) than in its surroundings. The lobe emission has an average spectral index $\alpha_5^{15} \sim 1.0$, the hot spot having the flattest spectrum ($\alpha = 0.7$). The projected magnetic field in the nucleus and the southern jet is directed parallel to the source axis. At 5 GHz the core and the jet are 11 and 3.4% polarized, respectively. At the position of the hot spot, the polarization rises sharply, to 5.9%. The level of polarization is highest on the west side of the hot spot, where the electric vectors are oriented perpendicular to the jet direction. On the east side, the degree of polarization drops sharply, and the magnetic field becomes more circumferential, following the contours of the brightness distribution. In the 5 GHz map, a blob of diffuse emission is present to the northwest of the core. This weak, irregular structure is not detected in the 15 GHz map, and hence of steep spectrum ($\alpha \geq 2.0$). The northern lobe is weakly polarized at 5 GHz; the direction of the magnetic field is circumferential.

The most remarkable feature in the 5 GHz intensity map is the blob of emission located $\sim 5''$ to the northwest of the nucleus, halfway to the northern lobe. The intensity of the northwestern blob is about six times the rms noise level in the 5 GHz map; we therefore believe the feature to be real. The probability of it being an unrelated background source is very small. The position of the blob suggests that it is part of a counterjet extending to the northwestern lobe. This would make 1317+520 a most unusual source, since two-sided jet emission is hardly ever observed in powerful quasars. A peculiar feature of the northwestern blob, however, is its steep radio spectrum: $\alpha_5^{15} \geq 2$, which is unusually high for a knot in a radio jet. It is somewhat mystifying that the blob itself has remained undetected in the 1.4 GHz map of Hintzen et al. (1983), whereas the lobe emission, which at 5 GHz is weaker, is clearly visible at 1.4 GHz. The spectrum of the jet thus should be much steeper than that of the lobe, which is rarely or never observed in quasars. The interpretation of the northwestern blob in terms of counterjet emission therefore remains somewhat doubtful. More sensitive observations of longer duration will be required to settle the issue.

3.5. 1548+114

The optical identification of this radio source is not entirely certain. On photographic plates, two optical objects are visible near the position of the radio nucleus: the close quasar pair 1548+114A (at redshift 0.436) and 1548+114B (at redshift 1.901), located at distances of 2 and 5″ from the radio core, respectively. The QSO closest to the radio nucleus, 1548+114A, has been assumed to be the optical object associated with the radio emission.

(*a*) *Mas-scale radio structure*: The nucleus of 1548+114 is one of the weakest in our sample; it has a flux density close to the limits of mapping with the Mk II recording system. Global fringe fitting has been applied to this source.

The derived VLBI hybrid map of the mas structure is presented in Fig. 5a. Most of the nuclear flux is contained within one slightly resolved component, designated A in the map. A weak secondary feature B is present at ~ 1.5 mas to the northeast of A; but since the flux of B is close to the noise level of the map, its significance is questionable. Another reason to doubt the reality of feature B is the fact that the position angle of B with respect to A differs from that of the large-scale jet of 1548+114 by $\sim 65°$; in most lobe-dominated quasars the arcsec- and mas-scale radio emission tend to be closely aligned. The visibility amplitudes and closure phases on the short and intermediate baselines indicate that there is no resolved structure in the nucleus of 1548+114 on scales larger than 2–3 mas. Due to the low declination of 1548+114, data on the longest baselines cover a small time interval only and do not offer strong constraints on structure within 2–3 mas from the core.

(*b*) *Large-scale radio structure*: At 5 GHz, the radio structure of 1548+114 is double-lobed, with a knotty, straight jet extending

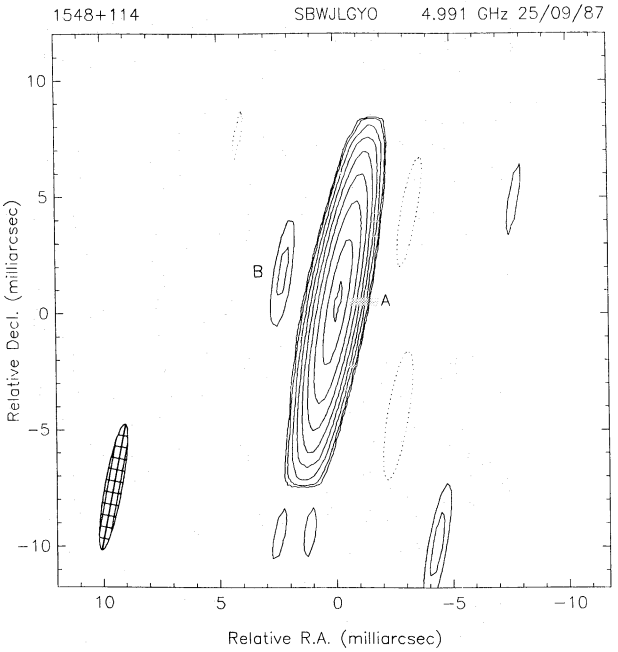

Fig. 5a. 5 GHz VLBI map of the total intensity I of 1548+114, observed at epoch 1987.73. The contour levels in the map are 1, 2, 4, 8, 16, 32, 64 and 96% of the peak flux value of 305 mJy per beam. The restoring beam is an ellipse of 3.5×0.7 mas, at a position angle of $-5°$

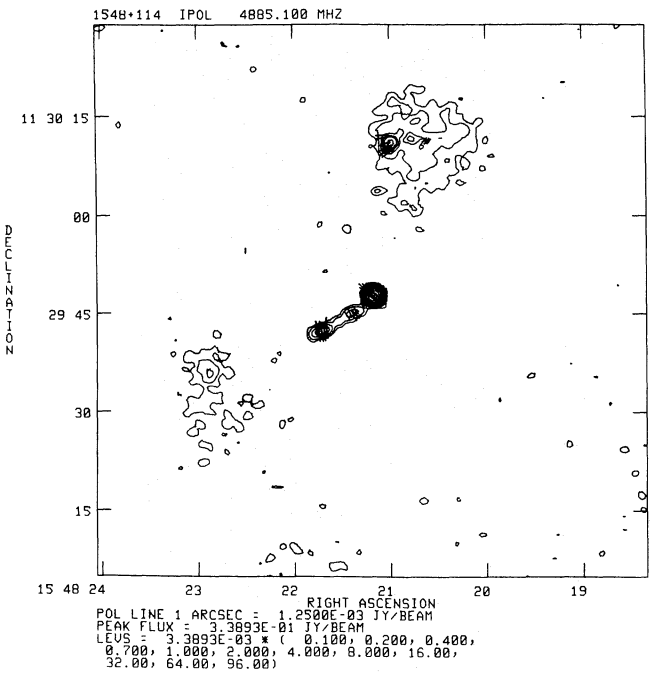

Fig. 5b. VLA map of the total intensity distribution I of 1548+114 at 5 GHz. The contour values in the map are 0.1, 0.2, 0.4, 0.7, 1, 2, 4, 8, 16, 32, 64 and 96% of the peak flux value of 338.9 mJy per beam. Superimposed on the contour plot are the electric vectors of the linearly polarized emission P, scaled in length to the intensity of P. An electric vector 1″ in size corresponds to a polarized flux density of 1.25 mJy per beam

to the southeast of the core (Fig. 5b). The lobe emission is weak and of steep spectrum on both sides of the nucleus. In the 15 GHz map, which is not shown here, there is no detectable jet or lobe emission; the observed intensities imply a flat spectrum for the core ($\alpha = 0.35$), and lower limits for the spectral indices of the jet and the southern and northern lobe (respectively, 1.5, 2.0 and 2.0).

The polarization of the core and southern lobe of 1548+114 in the 5 GHz map is negligible. Only at the two knots in the radio jet and in the northwestern hot spot does the degree of linear polarization rise above the noise level. The projected magnetic field in the jet is oriented parallel to the source axis. In the hot spot the polarization vectors are circumferential.

3.6. 1830+285

(*a*) *Mas-scale radio structure*: The VLBI hybrid map (Fig. 6a) obtained in June 1986 shows the mas-scale emission to have a resolved core–jet morphology. Several components can be distinguished, oriented along a position angle of $-43 \pm 3°$, and aligned with the kpc-scale jet to within 5°. The brightest, eastern component A is assumed to be the radio core. Two other components, designated B and C, are located at distances of 2.1 and 3.9 mas from A, respectively. No emission has been detected to the east of A.

(*b*) *Large-scale radio structure*: The VLA data for this quasar are presented in Fig. 6b, c. Both 5 and 15 GHz maps show a triple structure, with a knotty, discontinuous and slightly curved radio jet leading up to the northwestern lobe. The morphology of this lobe emission is complex (Fig. 6d, e). It contains a bright primary hot spot at the end of the jet and a weaker secondary emission peak to the north. More diffuse emission is also present to the southwest of the primary hot spot. The southeastern radio lobe contains a single central condensation.

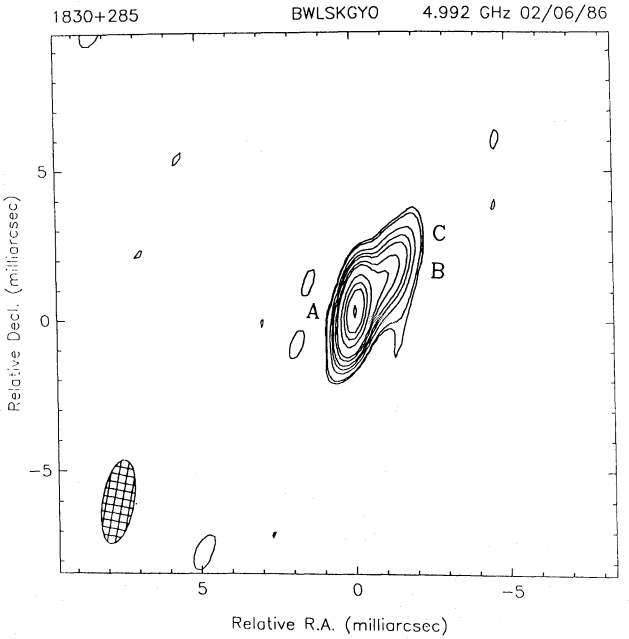

Fig. 6a. 5 GHz VLBI map of the total intensity I of 1830+285, observed at epoch 1986.42. The contour levels in the map are 0.5, 1, 2, 4, 8, 16, 32, 64 and 96% of the peak flux value of 309 mJy per beam. The restoring beam is an ellipse of 2.8 × 1.2 mas, at a position angle of −4°

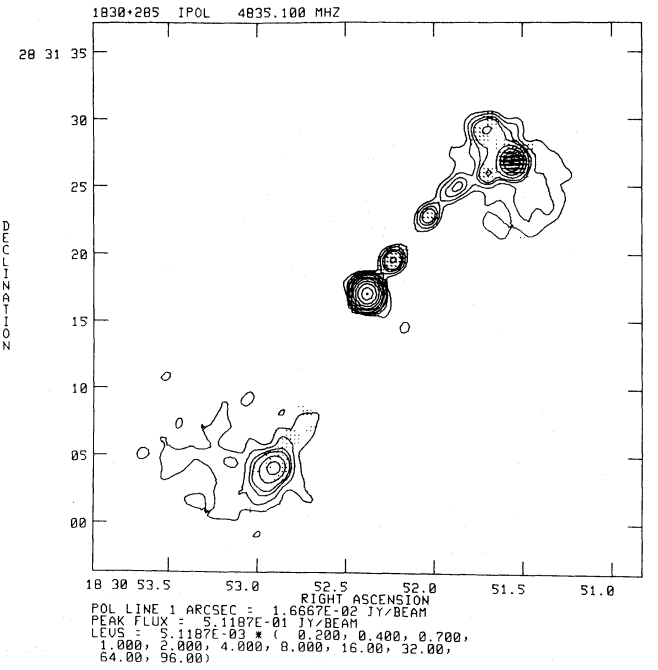

Fig. 6b. VLA map of the total intensity distribution I of 1830+285 at 5 GHz. The contour values in the map are 0.2, 0.4, 0.7, 1, 2, 4, 8, 16, 32, 64 and 96% of the peak flux value of 511.9 mJy per beam. Superimposed on the contour plot are the electric vectors of the linearly polarized emission P, scaled in length to the intensity of P. An electric vector 1″ in size corresponds to a polarized flux density of 16.7 mJy per beam

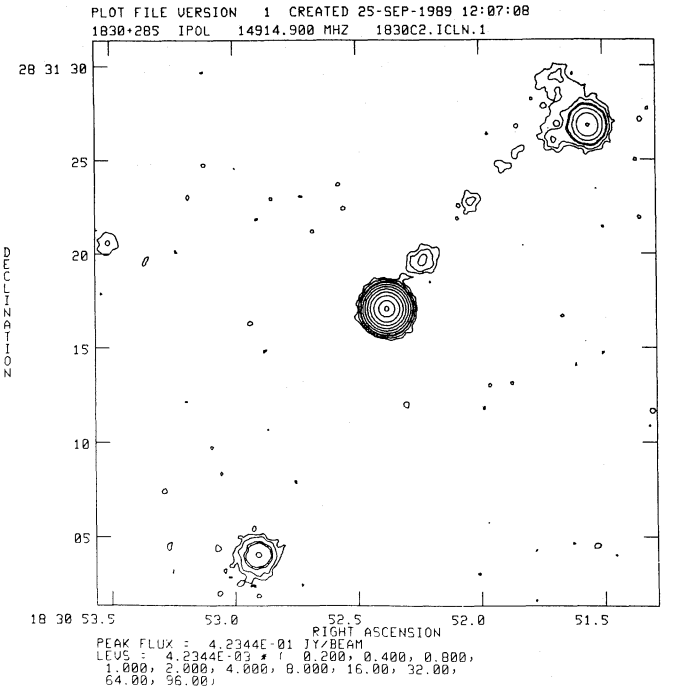

Fig. 6c. VLA map of the total intensity distribution I of 1830+285 at 15 GHz. The contour values in the map are 0.2, 0.4, 0.8, 1, 2, 4, 8, 16, 32, 64 and 96% of the peak flux density of 423.4 mJy per beam

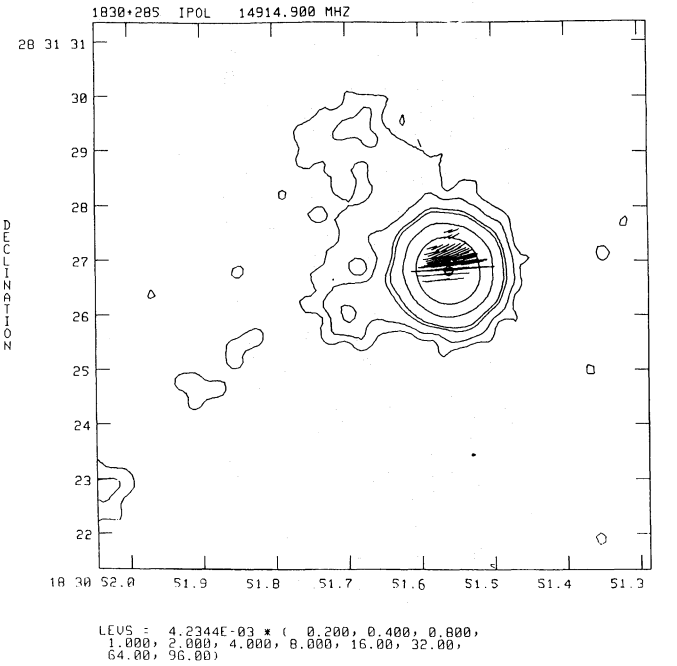

Fig. 6e. The total intensity distribution I and polarization vectors in the north-western hot spot of 1830+285 at 15 GHz. The contour values are the same as in Fig. 6b. A polarization vector 1″ in size corresponds to a polarized flux density of 5.0 mJy per beam

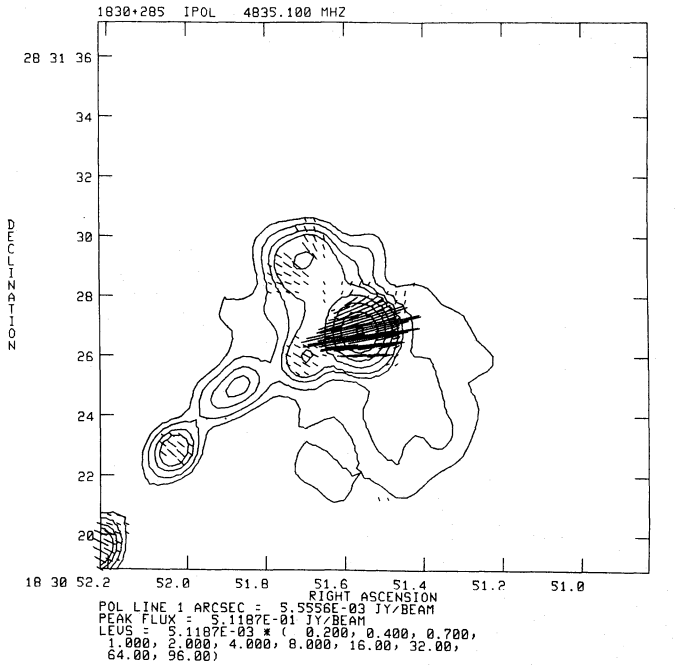

Fig. 6d. The total intensity distribution I and polarization vectors in the north-western hot spot of 1830+285 at 5 GHz. The contour values are the same as in Fig. 6a. A polarization vector 1″ in size corresponds to a polarized flux density of 11.1 mJy per beam

The nucleus of 1830+285 has a fairly flat radio spectrum (α_5^{15} = 0.3), and no significant linear polarization. The one-sided jet structure consists of several knots of emission, forming a curved trajectory between core and primary hot spot. The spectral index of the knots lies in the range 0.5–1.0. The blobs are unresolved in the direction transverse to the jet; but in their longitudinal direction the angular resolution is sufficient to observe a gradient in spectral index over the length of the blobs. In three of the four knots the spectrum within the knots is steepest on the side of the nucleus (0.9–1.0, as compared to 0.5–0.6 on the opposite side). This type of spectral behaviour is predicted in several models of discrete blob emission and of continuous hydrodynamic jets (e.g. Begelman et al. 1984).

The structure of the northwestern lobe has been highlighted in Fig. 6d, e. This region is the only part of 1830+285 which is significantly polarized at either 5 or 15 GHz. Most of the linearly polarized flux is emitted at the location of the primary hot spot. The projected magnetic field in the hot spot is oriented mainly perpendicular to the radio jet axis, at both 5 and 15 GHz.

At 5 GHz, the northern lobe emission contains three substructures: the primary hot spot, the secondary peak to the northwest and diffuse emission to the southwest. In the 15 GHz only the first two features are present; the southwestern emission has a very much steeper spectrum ($\alpha \geq 2.0$). The primary hot spot is unresolved. The ridge of emission between it and the secondary peak is oriented nearly perpendicular to the radio jet, which terminates at the primary hot spot. The observed morphology is suggestive of a redirection of the jet flow at the position of the primary hot spot towards the secondary peak. The flow appears to be deflected over an angle of nearly 120°.

3.7. 2209+080

(*a*) *Mas-scale radio structure*: Snapshot VLBI observations made in October 1984 indicated the presence of resolved structure on mas scales. However, between this epoch and the 6 h

observing run in June 1986, the radio intensity of 2209+080 declined drastically: the total 5 GHz flux density (determined from single-dish measurements by the Effelsberg telescope) dropped by ~40% from 1.1 to 0.85 Jy; the core flux density (defined as the maximum correlated flux density on the shortest VLBI baseline) decreased by ~60% fom 300 to 135 mJy. Much phase noise was present in the 1986 data. Even after application of global fringe fitting, the source remained undetected on most baselines. This suggests that the mas-scale structure of 2209+080 is rather diffuse and extended. To obtain a more reliable map of this radio core in its present low-flux state, use of the more sensitive Mk III recording equipment will be required.

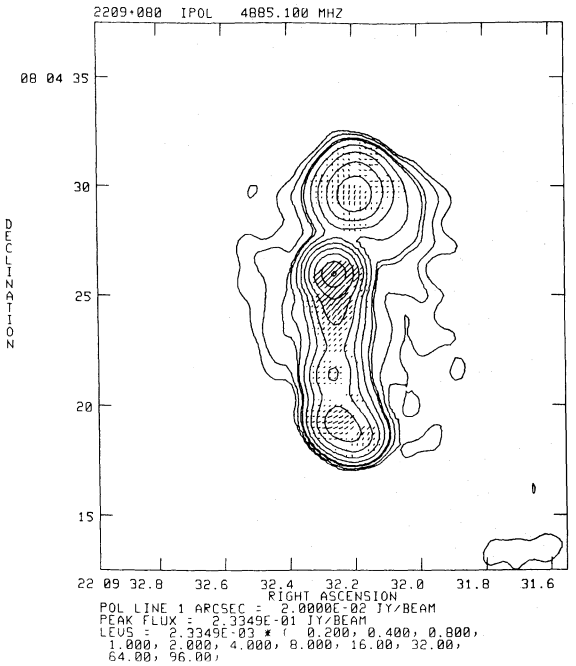

Fig. 7a. The total intensity distribution I of 2209+080 at 5 GHz. The contour values in the map are 0.2, 0.4, 0.8, 1, 2, 4, 8, 16, 32, 64 and 96% of the peak flux value of 233.5 mJy per beam. Superimposed on the contour plot are the electric vectors of the linearly polarized emission P, scaled in length to the intensity of P. An electric vector 1″ in size corresponds to a polarized flux density of 20 mJy per beam

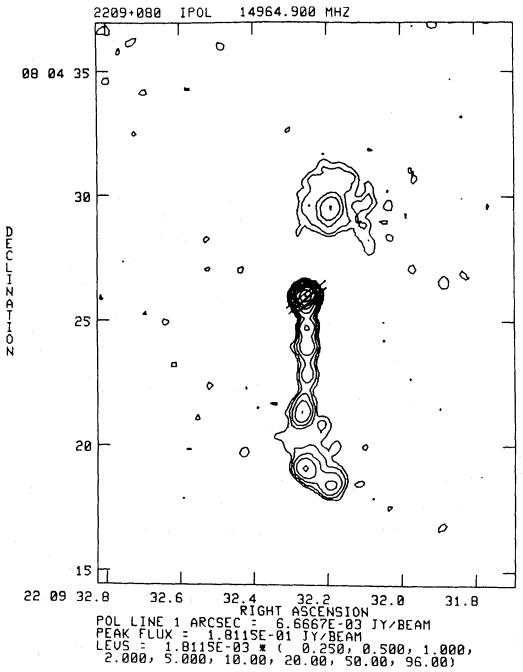

Fig. 7b. The total intensity distribution I of 2209+080 at 15 GHz. The contour values in the map are 0.25, 0.5, 1, 2, 4, 8, 16, 32, 64 and 96% of the peak flux density of 181.2 mJy per beam. Superimposed on the contour plot are the electric vectors of the linearly polarized emission P, scaled in length to the intensity of P. An electric vector 1″ in size corresponds to a polarized flux density of 6.7 mJy per beam

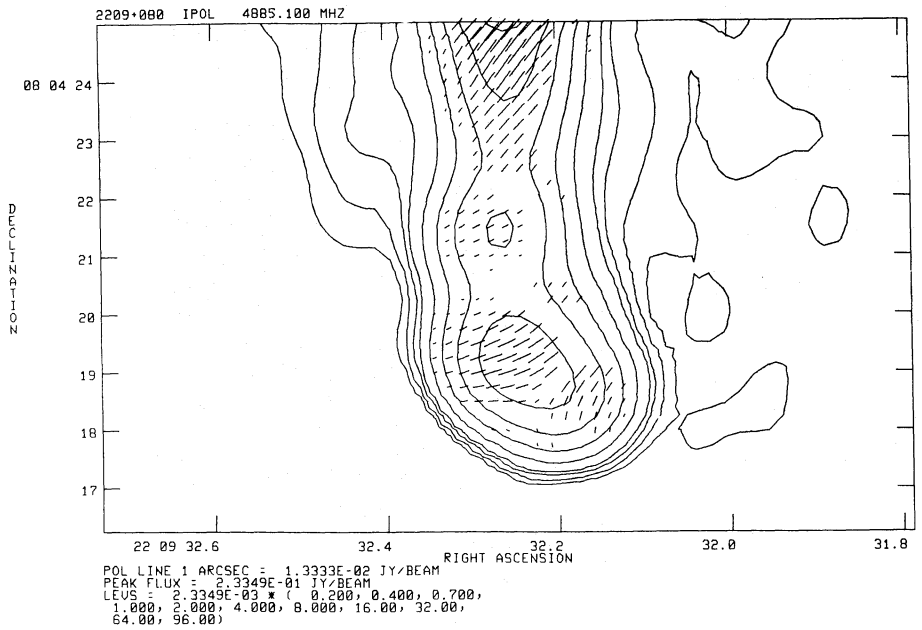

Fig. 7c. The total intensity distribution I and polarization vectors in the southern hot spot of 2209+080 at 5 GHz. The contour values are the same as in Fig. 7a. A polarization vector 1″ in size corresponds to a polarized flux density of 13.3 mJy per beam

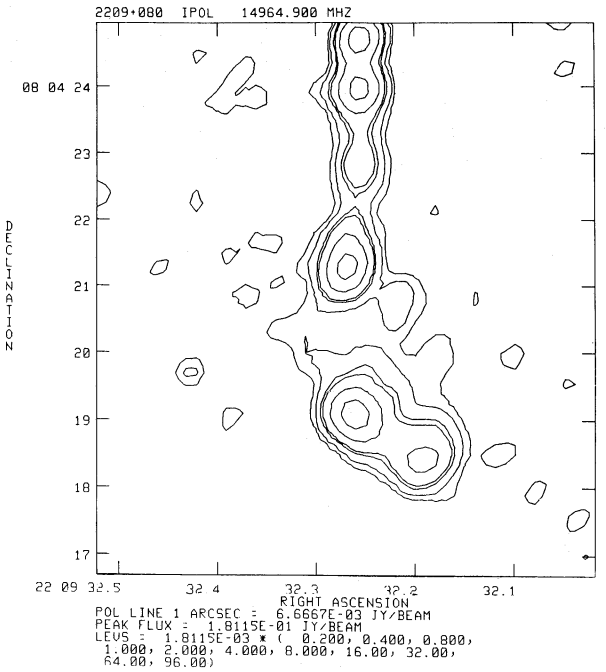

Fig. 7d. The total intensity distribution I and polarization vectors in the southern hot spot of 2209+080 at 15 GHz. The contour levels in the map are 0.2, 0.4, 0.8, 1, 2, 4, 8, 16, 32, 64 and 96% of the peak flux value of 181.2 mJy per beam

(*b*) *Large-scale radio structure*: The radio structure associated with this quasar is shown in Fig. 7a, b. The triple morphology is aligned nearly north-south, with a prominent jet extending to the southern lobe. In the 5 GHz map the southern jet is continuous and fairly smooth; the flux density ratio between the jet and the emission to the north of the core is low (~ 4). The 15 GHz map, on the other hand, shows a strongly asymmetric radio source, with a jet–counterjet flux density ratio ≥ 90, and a considerable amount of structure in the southern jet. The jet emission extends southwards out to a distance of 7″ from the core. At that point it terminates in a double hot spot structure (Fig. 7c, d). The jet is directed towards the brightest, eastern peak. The ridge of emission connecting the primary and secondary hot spots is directed to the southwest, along an angle of 50° with respect to the jet axis. The primary hot spot emission is elongated slightly in the direction of the secondary peak.

At 5 GHz the integrated degree of linear polarization in 2209+080 is 5.6%. Most of the linearly polarized emission is concentrated in the unresolved nucleus. The polarization of jet and lobes is considerably weaker ($\leq 2.0\%$). The electric vectors are oriented mainly along the direction of the radio jet. At 15 GHz the nuclear emission is 1.2% linearly polarized. Outside the core the level of polarization is negligible.

On the whole the spectral index α_5^{15} steepens gradually from the flat spectrum ($\alpha = 0.2$) core along the jet to the southern lobe. The increase in α is not monotonic, since the spectrum flattens noticeably at the positions of the knots in the jet visible in the 15 GHz map. The gradual steepening of the spectrum away from the core is consistent with spectral ageing of the radiating relativistic electrons; the relatively flat spectrum at the positions of the knots in the jet and the two hot spots is an indication of particle reacceleration "in situ" at these points.

As in the case of 1830+285, the morphology and spectral behaviour of the double hot spot structure suggests that, at reaching the primary hot spot, the radio jet has collided with, and been deflected by, dense intervening matter. The abrupt change in direction of the radio emission, the elongation of the primary hot spot towards the secondary, and the steeper spectrum of the secondary are all consistent with this interpretation.

3.8. 2251+134

(*a*) *Mas-scale radio structure*: Full-track VLBI observations of this optically faint quasar were first obtained in September 1985; but since in this experiment no less than four of the eight available stations failed, the source was re-observed in June 1986. In this run, source switching took place between 2209+080 and 2251+134, resulting in a considerable loss of information in the *uv*-plane. The quantity of data was further diminished by the poor playback performance of a number of data tapes. Also, the visibility data do not show clear maxima or minima. The data therefore do not offer enough restrictions to allow an accurate mapping of any structure of great complexity.

The closure phases, which are offset from the zero level, indicate the presence of asymmetric mas-scale radio structure in the nucleus of 2251+134. The cleaned map, displayed in Fig. 8a, shows a resolved, asymmetric three-component structure approximately 4 mas in angular extent. The westernmost, brightest component contains $\sim 75\%$ of the flux on the shortest baselines. The two other components are of nearly equal flux density and positioned at distances of 1.4 and 2.8 mas to the east of the peak flux density position. The three-component "core–jet" structure is aligned to within 10° with the large-scale radio emission. Assuming that the brightest component in the VLBI

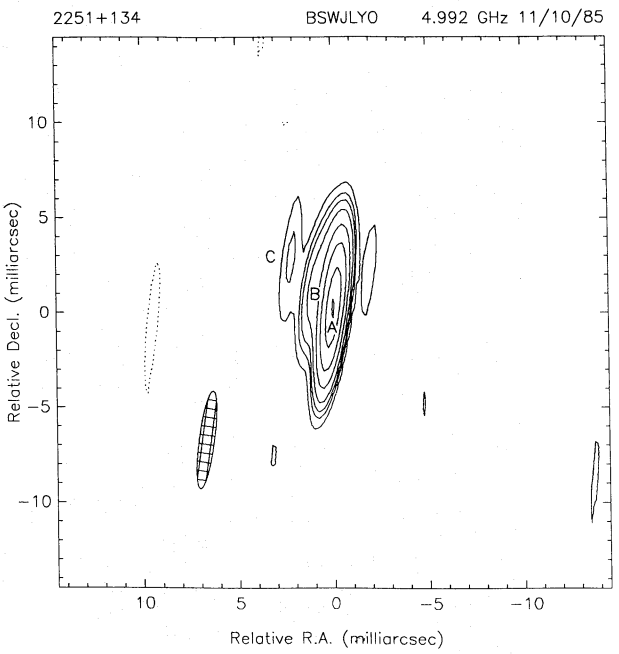

Fig. 8a. 5 GHz VLBI map of the total intensity I of 2251+134, observed at epoch 1986.42. The contour levels in the map are 1, 1.5, 2, 3, 4, 8, 16, 32, 64 and 96% of the peak flux value of 370 mJy per beam. The restoring beam is an ellipse of 4.0×0.6 mas, at a position angle of $-5°$

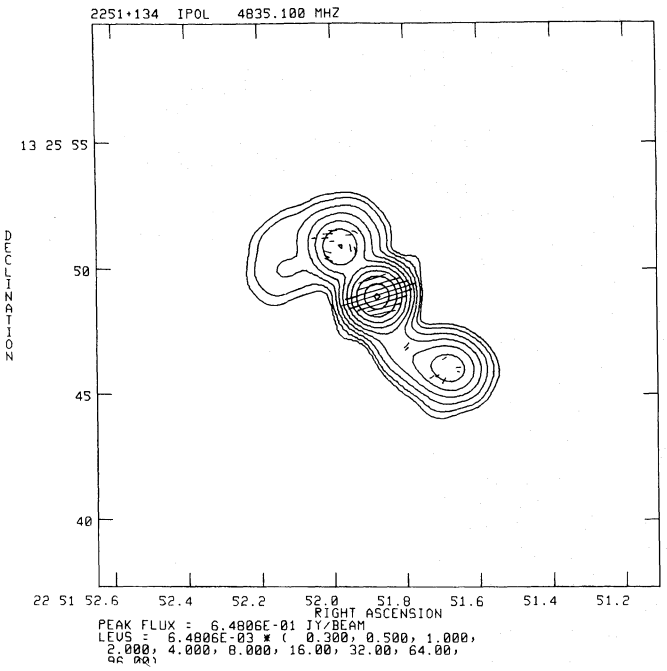

Fig. 8b. The total intensity distribution I of 2251+134 at 5 GHz. The contour values in the map are 0.3, 0.5, 1, 2, 4, 8, 16, 32, 64 and 96% of the peak flux value of 648.1 mJy per beam. Superimposed on the contour plot are the electric vectors of the linearly polarized emission P, scaled in length to the intensity of P. An electric vector 1″ in size corresponds to a polarized flux density of 4.9 mJy per beam

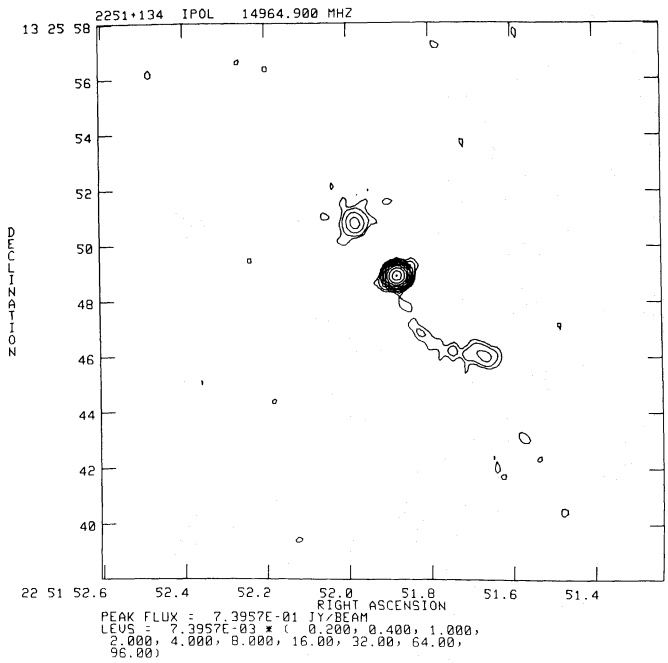

Fig. 8c. The total intensity distribution I of 2251+134 at 15 GHz. The contour values in the map are 0.3, 0.5, 1, 2, 4, 8, 16, 32, 64 and 96% of the peak flux density of 730.2 mJy per beam

map represents the quasar core, the mas-scale jet of 2251+134 is pointing in the direction *opposite* to that of the overall radio morphology (see below). If confirmed, this would make 2251+134 an unusual object among lobe-dominated quasars, in which the mas-scale emission normally is pointing in the same direction as the large scale jet to within a few degrees. VLBI observations at another frequency are required to establish the location of the radio nucleus, and hereby the direction of the VLBI "jet", definitely.

(*b*) *Large-scale radio structure*: The quasar 2251+134 is associated with a relatively small triple radio source (~13″ in angular extent), having a bright, dominant radio core. At 5 GHz (Fig. 8b), the overall morphology is somewhat Z-shaped: the northeastern emission apparently bends rather abruptly through nearly 90° towards the east at a location 2.5″ distant from the core, while the southwestern structure curves more gradually to the west.

The 15 GHz map (Fig. 8c) displays a weak curved jet extending to, and terminating at, the southwestern intensity peak. The spectrum of both jet and lobe emission is rather steep: $\alpha_5^{15} \geq 1.5$. The northeastern emission at 15 GHz consists only of the compact feature 2.5″ away from the core (which has an average spectral index $\alpha \sim 1.0$). The additional structure towards the east that was apparent in the 5 GHz data is not visible here. The absence of the eastern emission in the 15 GHz map implies that the radio spectrum in this region is steep: $\alpha \geq 1.5$. The integrated degree of linear polarization in 2251+134 at 5 GHz is 3.2%. Most of the polarized radiation is emitted by the core; jet and lobes are only marginally polarized. At 15 GHz, the polarized emission was very weak and noisy.

4. Comparison of pc- and kpc-scale radio jets

In all sources except 1055+201 jet emission of kpc-scale dimensions is observable at 5, and sometimes at 15 GHz. The large-scale jet structures usually appear to be one-sided. Only in the case of 1317+520 is there any indication of the presence of counterjet emission above the noise level; but the identification of the feature to the northwest of the core of 1317+520 as being part of a counterjet remains doubtful.

The level of linear polarization at 5 and 15 GHz generally was low, a few percent at most. For the six sources for which polarization maps were derived, the polarized flux densities were too low to permit a determination of the degree of depolarization of the various substructures in the maps.

On mas scales, the nucleus of 1548+114 appears to be unresolved, that of 1055+201 has a symmetric appearance, and that of 2209+080 is too weak to be mapped. The cores of the remaining five quasars, 0850+581, 1222+216, 1317+520, 1830+285 and 2251+134 display an asymmetric core–jet structure similar to the morphologies observed in more core-dominated objects. The nuclear structures in the extended quasars sources usually point in the direction of the kpc-scale radio jet; the elongated nuclear emission is well aligned (to within 10°) with the overall radio morphology. The exception is 2251+134, in which the nuclear emission is directed opposite to the outer jet structure (assuming that the brightest feature in the VLBI map represents the radio core).

Four of the eight quasars possess highly curved or distorted large-scale jets: 0850+581, 1222+216, 1317+520 and 2251+134. For these sources, the behaviour of the nuclear emission on one hand, and the outer radio structure on the other, is consistent with a gradual and continuous bending of the jet from pc to kpc scales. In all objects, the position angles of the secondary VLBI components correspond closely to that of the *inner* part of the kpc-scale jet.

The distorted overall structures of the quasars 0850+581, 1222+216 and 2251+134 suggest that the radio jets in these objects may be precessing. In the highly distorted source 1222+216, the jet bends continuously over an angle of more than 130° from the nucleus to the eastern lobe [compare Fig. 3a to the VLA map of Hintzen et al. (1983)]. In terms of precession models, this high degree of curvature is consistent with a geometry in which the jet axis is inclined close to the line of sight.

In the cases of 0850+581 and 1317+520, the VLBI maps show that the curvature of the radio jet sets in within a few parsecs of the core. The nuclear radio emission of 0850+581 (Fig. 1a) shows a wiggly structure which resembles the "corkscrew" morphology of the large-scale radio jet (Shone 1985; Browne 1987). In 1317+520, the mas-scale "jet" emission appears to bend in a direction opposite to that of the kpc-scale radio jet; this observation lends support to the suggestion that in this source, too, the radio structure may be affected by jet precession.

5. Hot spot emission and jet velocity

The asymmetric jet morphologies generally observed in quasars on both pc and kpc scales are consistent with the presence of relativistic motions throughout the radio jets. In view of the potentially great influence of the velocity of the radio-emitting material on the radiative properties of a source, it is evidently of great interest to obtain independent estimates of the velocities in jets at all length scales. Expansion speeds close to the nucleus are usually estimated from VLBI proper motion studies, although the interpretation of these structural changes on pc scales in terms of material motion is by no means certain. It is more difficult to obtain estimates of the jet velocity closer to the outer lobes. One indirect measure of the order of magnitude of the jet material speed can be obtained from observations of quasar hot spots. Hot spots are believed to be the locations where the radio jet terminates and dumps the bulk of its kinetic energy. Under the assumption of dynamical equilibrium between jet and hot spot, the observed luminosity and energy density of the hot spot emission can be used to place constraints on the velocity of the jet and the momentum carried by it.

Let us consider a situation in which the radio jet is in pressure balance with the hot spot:

$$\rho_j(\gamma_j v_j)^2 = \frac{u_{hs}}{3}, \tag{1}$$

where ρ_j is the jet density in the comoving frame, v_j the velocity of the working surface of the jet at the hot spot position, γ_j the accompanying Lorentz factor and u_{hs} the energy density internal to the hot spot. For u_{hs} we adopt the minimum energy value. The hot spots are assumed to be spherical in shape and uniformly filled. Since the hot spots of all sources observed by us are unresolved, we will assume a typical hot spot radius of 0.1 kpc; VLBI observations of several compact hot spot structures by Lonsdale & Barthel (1984, 1986) have yielded radii of this order of magnitude. We will further assume that the jet deposits its bulk kinetic energy into the hot spot region, where it is converted into radio emission at some efficiency $\varepsilon < 1$. This results in an energy balance of the form

$$L_j = \frac{L_{hs}}{\varepsilon} = \pi r_j^2 \rho_j v_j c^2 \gamma_j(\gamma_j - 1), \tag{2}$$

where L_j and L_{hs} are the kinetic power of the jet and the hot spot radio luminosity, respectively, and r_j is the radius of the jet. Combining Eqs. (1) and (2) and eliminating ρ_j, we find the efficiency of conversion from kinetic to radio energy to be

$$\varepsilon = 3.18\ 10^{-11} \frac{L_{hs}}{u_{hs} r_j^2} \left(\frac{\gamma_j + 1}{\gamma_j - 1}\right)^{1/2}, \tag{3}$$

where the units of L_{hs}, u_{hs} and r_j are 10^{43} erg s^{-1}, erg cm^{-3} and kpc, respectively.

The efficiency factor ε takes into account, among other effects, the fact that a certain fraction of the jet energy is not radiated away at the hot spot position, but gives rise to the diffuse radio lobes. Thus, we essentially adjust for the presence of the lobe emission through the correction factor ε. An alternative approach would be to apply the luminosity and energy density of the entire lobe emission in Eq. (3), rather than the values of L_{hs} and u_{hs} for the hot spot alone. Since for the sources under consideration here the overall lobe emission is dominated by the hot spots, these two methods yield quantitatively similar results. The major source of uncertainty lies in the (unknown) efficiency by which the jet energy is converted into radiation. The accuracy of our estimate for this conversion factor, which is included in ε, determines the accuracy of the jet velocity estimates derived by the model.

A lower limit to the efficiency ε of the energy conversion is obtained by considering the maximum possible values of γ_j and r_j: $\gamma_j = \infty$ and $r_j = r_{hs}$. For the three quasars in our sample having the most pronounced hot spot emission (1055+201, 1830+285 and 2209+080), the calculated values of ε_{min} range between 0.01 and 0.15 (Table 5).

Assuming a maximum efficiency ε of 1, Eq. (3) yields a lower limit to γ_j and v_j. For the three sources involved, minimum jet velocities ranging from 0.33 to 0.65c are obtained. Actually, the maximum possible value of ε is likely to be well below unity, as not all of the kinetic energy will be converted to radiative energy. Thus, the given lower limits to v_j are probably underestimates. Gopal-Krishna & Saripalli (1984) argue that a reasonable upper limit for ε in powerful double radio sources is given by $\varepsilon_{max} = 0.3$. Using this value, we derive minimum jet velocities ranging from 0.57 to 0.92c (Table 5).

On the basis of this simple model, therefore, we conclude that, close to the hot spots, the flow velocities of the quasar jets are relativistic. In extended quasars with bright radio cores, such as the ones studied here, highly relativistic motion is commonly detected on mas scales (Impey 1987; Cohen et al. 1988). Depolarization measurements by e.g. Garrington et al. (1988) and Laing (1989) indicate that the jets in these objects are likely to retain most of their kinetic energy as far out as the radio lobes. One would therefore expect to find relativistic motions in the hot spot

Table 5. Physical parameters of hot spot sources

Source	1055+201	1830+285	2209+080
u_{hs} (10^{-9} erg cm^{-3})	9.9	2.4	0.9
L_{hs} (10^{43} erg s^{-1})	2.2	1.0	0.8
ε_{min}	0.07	0.13	0.03
γ_{min} ($\varepsilon_{max}=1$)	1.15	1.30	1.06
β_{min} ($\varepsilon_{max}=1$)	0.49	0.64	0.33
γ_{min} ($\varepsilon_{max}=0.3$)	1.60	2.5	1.22
β_{min} ($\varepsilon_{max}=0.3$)	0.78	0.92	0.57

regions of superluminal triple quasars. The kinematical model presented here, however crude, is consistent with this prediction.

6. Discussion

In the context of a study of the structural evolution within the nuclei of large double-lobed quasars, we have obtained first epoch VLBI maps of eight quasars with extended radio structure. For five of the eight sources shown here, the VLBI data yielded maps of good quality. In one quasar, 2209+090, the core flux density at the time of observation had dropped below the level at which Mk II observations can produce reasonable signal-to-noise maps. For two other sources, the quasars 1055+201 and 2251+134, the data were of low quality due to a large loss of data and a consequently inadequate *uv*-coverage.

The most well-known source in our sample is the quasar 0850 +581, for which Barthel et al. (1986) have reported the occurrence of superluminal motion. Our 5 GHz map confirms the structure and expansion velocity found by Barthel et al. Clear multi-component structure was detected in the nuclei of 1222+216, 1317+520 and 1830+285 as well. The relative flux densities of the nuclear components in these objects indicate that the mas-scale radio emission is one-sided. In the quasar 1548+114 no resolved nuclear radio emission was detected, in contrast to expectations based on an earlier pilot survey (Barthel et al. 1984). Of the two sources with low quality VLBI maps, 1055+201 is a candidate source for symmetrical nuclear structure, while 2251 +134 appears to have a more conventional core–jet morphology.

The multi-component structures present in five of the observed extended quasars designate these sources as candidates for proper motion studies. The nuclei of the quasars 1222+216 and 1830+285 have later been reobserved at 5 GHz. Indications for the presence of superluminal motion were found in both cases (Hooimeyer et al. 1991); mapping at a third epoch is required to confirm the observed proper motion values. The nuclei of the sources 1317+520 and 2251+134 have not yet been re-observed. Because of its multi-component nuclear structure, the former is a good candidate for further VLBI monitoring. The nucleus of 1317 +520 is at the lower edge of the flux density range for which Mk II observations yield reliable maps; it would therefore be preferable to perform future VLBI observations of this source with Mk III networks.

In all, VLBI monitoring of the 13 extended quasars in our sample for which the initial pilot surveys (Barthel et al. 1984, HBSM) indicated the presence of resolved nuclear emission, has led by now to three confirmed cases of superluminal motion: 0850 +581 (Barthel et al. 1986), 1137+660 (Hough & Readhead 1987) and 1721+343 (Barthel et al. 1989; Hooimeyer et al. 1991). In two other candidates, 1222+216 and 1830+285, the observed proper motions indicate superluminal velocities (Hooimeyer et al. 1991), but these results remain to be confirmed. The observed velocities in all cases are in the range of 1–3*c*, moderate values compared to those found in more core-dominated objects.

VLA observations were made for six of the eight lobe-dominated quasars at 5 and 15 GHz. Polarization images and spectral index maps were obtained for most objects. Energy density, magnetic field strength and velocity estimates were derived for the various components in each source. The misalignment between the nuclear emission and the inner part of the kpc-scale radio jet is small in all cases except 2251+134, where the VLA and VLBI jets appear to be oppositely directed. The overall structure of the distorted sources 0850+581, 1222+216 and 2251 +134 is suggestive of precession of the radio jet. A comparison between the curved emission on pc and kpc scales in the quasar 1317+520 shows that the morphology of this source is compatible with precession models as well.

In several sources a well-defined, sometimes double, hot spot structure was present. The kinematical model of this hot spot emission described in Sect. 5, implied relativistic motions to be present in those regions. Within the context of the simple relativistic beaming model, the inferred high velocity values are consistent with the jet–counterjet flux density asymmetric observed on kpc scales; they are in conflict, however, with the symmetric appearance of the lobe structure (in terms of both flux density and separation from the core) in these lobe-dominated quasars.

In roughly 1/3 of the large double quasars under consideration here, evidence for moderately superluminal expansion was found, implying the presence of relativistic motions close to the quasar nuclei. Observations of lobe-dominated quasars from other samples (e.g. Hough & Readhead 1987, 1989; Zensus & Porcas 1986) yield similar results. The superluminal expansion velocities detected in a large fraction of the lobe-dominated quasars that have been monitored to date, imply these objects to be inclined at relatively small angles to the line of sight, in spite of their large projected radio sizes. If the sources for which proper motions have been determined so far are representative for the quasar population as a whole, then the simple relativistic beaming model as formulated by Orr & Browne (1982) is clearly inconsistent with the data. A better agreement with the observations is then obtained by a modified version of the beaming model, in which quasars are proposed to be powerful double-lobed radio galaxies inclined close to the line of sight (Scheuer 1987; Barthel 1989).

Nevertheless, one should keep in mind that the observations available at present give us an incomplete, and possibly highly misleading, picture of the distribution of apparent velocities in quasar nuclei. The few double-lobed quasars that have been studied in detail, all possess relatively bright radio cores. The double-lobed quasars with truly weak nuclear radio emission, in which subluminal motion is much more likely to occur, and far more difficult to observe, and may not be accessible to VLBI networks for some time. Also, many lobe-dominated sources have simply not yet been monitored sufficiently long to definitely establish proper motions. At the presently attainable resolutions, the detection of subluminal motion in an intermediate redshift ($z \sim 0.5$–1.0) quasar requires a monitoring period of 10 yr or more; few lobe-dominated sources have been studied this long. The observed distribution of apparent velocities is therefore subject to a heavy bias against the inclusion of subluminal sources. It is significant that, as time has progressed, ever lower apparent velocities have been detected in ever weaker nuclei. Patient monitoring of weak radio cores might well reveal the presence of a large population of subluminal quasars, which hitherto has been impossible to detect.

With the coming of age of the very large baseline array (VLBA), routine monitoring of large samples of objects with relatively weak radio cores over a period of 10 yr or more, has become a possibility. An observing program dedicated to this purpose, however unspectacular and lacking results in the short run, will provide us with essential information on the true

distribution of apparent velocities in quasar nuclei and should be given high priority.

Acknowledgements. We thank the staff at the telescopes involved in this experiment for their assistance with the observations, and the correlator staff at the California Institute of Technology for their help with the data processing. We gratefully acknowledge the assistance of Joris Blommaert in the reduction of the data. The NRAO VLA is operated by Associated Universities Inc., under contract with the National Science Foundation. The Netherlands Foundation for Research in Astronomy is supported by the Netherlands Organization for Scientific Research (NWO).

References

Barthel P.D., 1987, in: Pearson T.J., Zensus J.A. (eds.) Superluminal Radio Sources. p. 148
Barthel P.D., 1989, ApJ 336, 606
Barthel P.D., Miley G.K., Schilizzi R.T., Preuss E., 1984, A&A 140, 399
Barthel P.D., Miley G.K., Schilizzi R.T., Preuss E., 1985, A&A 151, 131
Barthel P.D., Pearson T.J., Readhead A.C.S., Canzian B. 1986, ApJ 310, L7
Barthel P.D., Hooimeyer J.R., Schilizzi R.T., Miley G.K., Preuss E., 1989, ApJ 336, 601
Begelman M.C., Rees M.J., Blanford R.D., 1985, Rev. Mod. Phys. 56, 255
Blandford R.D., Königl A., 1979, ApJ 232, 34
Browne I.W.A., 1987, in: Pearson T.J., Zensus J.A. (eds.) Superluminal Radio Sources. p. 129
Cohen M.H., Moffet A.H., Romney J.D., Schilizzi R.T., Shaffer D.B., Kellermann K.I., Purcell G., Grove G., Swenson G., Yen J.H., Pauliny-Toth I.I.K., Preuss E., Witzel A., Graham D., 1975, ApJ 210, 249
Cohen M.C., Barthel P.D., Pearson T.J., Zensus J.A., 1988, ApJ 333, 9
Garrington S.T., Leahy J.P., Conway R.G., Laing R.A., 1988, Nat 331, 147
Gopal-Krishna, Saripalli L., 1984, A&A 141, 61
Hewitt A., Burbidge G., 1980, ApJS 43, 57
Hewitt A., Burbidge G., 1987, ApJS 63, 1
Hintzen P., Ulvestad J.S., Owen F.N., 1983, AJ 88, 709
Hooimeyer J.R.A., Barthel P.D., Schilizzi R.T., Miley G.K., 1991, ApJ (submitted) (HBSM)
Hough D., Readhead A.C.S., 1987, ApJ 321, L11
Hough D., Readhead A.C.S., 1989, AJ 98, 1208
Impey C., 1987, in: Zensus J.A., Pearson T.J. (eds.) Superluminal Radio Sources, p. 233
Laing R.A., 1989, in: ESO Workshop, Extranuclear activity in galaxies. p. 52
Lonsdale C., Barthel P.D., 1984, A&A 135, 45
Lonsdale C., Barthel P.D., 1986, AJ 92, 1
Miley G.K., 1980, ARA&A 18, 165
Neff S.G., Brown R.L., 1984, AJ 89, 195
O'Dea C., Barvainis R., Challis P.M., 1988, AJ 96, 435
Orr M.J.L., Browne I.W.A., 1982, MNRAS 200, 1067
Owen F.N., Puschell J.J., 1984, AJ 89, 932
Pearson T.J., Readhead A.C.S., 1984, in: Fanti R., Kellermann K.I., Setti G. (eds.) Proc. IAU Symp. 110, VLBI and compact radio sources. p. 15
Scheuer P.A.G., 1984, in: Fanti R., Kellermann K., Setti G. (eds.) Proc. IAU Symp. 110, VLBI and compact radio sources. p. 197
Scheuer P.A.G., 1987, in: Zensus J.A., Pearson T.J. (eds.) Superluminal Radio Sources. p. 104
Scheuer P.A.G., Readhead A.C.S., 1979, Nat 277, 182
Schwab F.R., Cotton W., 1983, AJ 88, 688
Shone D., 1985, Ph.D. Thesis, Univ. of Manchester
Thompson A.R., Clark B.G., Wade C.M., Napier P.J., 1980, ApJ 44, 151
Zensus J.A., Porcas R.W., 1986, Swarup G., Kapahi V.K. (eds.) Proc. IAU Symp. 119, Quasars. p. 158